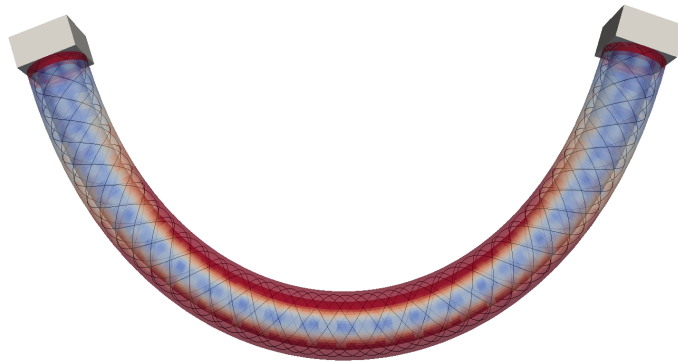




CHALMERS
UNIVERSITY OF TECHNOLOGY



Modeling of Steel Reinforced Flexible Hoses

Master's thesis at Fraunhofer Chalmers Centre

SHANKAR PARAMASIVAM

MASTER'S THESIS AT FRAUNHOFER CHALMERS CENTRE

Modeling of Steel Reinforced Flexible Hoses

SHANKAR PARAMASIVAM



CHALMERS
UNIVERSITY OF TECHNOLOGY

Department of Industrial and Materials Science
CHALMERS UNIVERSITY OF TECHNOLOGY
Gothenburg, Sweden 2019

Modeling of Steel Reinforced Flexible Hoses
SHANKAR PARAMASIVAM

© SHANKAR PARAMASIVAM, 2019.

Supervisor: Christoffer Cromvik, Fraunhofer-Chalmers Centre
Supervisor: Fredrik Andersson, Fraunhofer-Chalmers Centre
Examiner: Fredrik Larsson, Department of Industrial and Materials Science

Master's Thesis 2019
Department of Industrial and Materials Science
Chalmers University of Technology
SE-412 96 Gothenburg
Telephone +46 31 772 1000

Cover: Von Mises stress distribution on a rubber model of the reinforced hose in MeSOMICS bending simulation.

Printed by Chalmers Reproservice
Gothenburg, Sweden 2019

Modeling of Steel Reinforced Flexible Hoses
SHANKAR PARAMASIVAM
Department of Industrial and Materials Science
Chalmers University of Technology

Abstract

Steel reinforcements are commonly used to strengthen rubber hoses which are used in high pressure applications (in the field of engineering). Reinforced hoses become stiff when subjected to pressure. Thus, there is a requirement to model reinforcements which would predict the effect of stiffening. Modeling helically wounded reinforcements is the main focus of this work. Deformation of helically reinforced rubber hoses under pressure depend on the helix angle at which the reinforcement is laid around the hose.

The current study was carried out at Fraunhofer Chalmers Centre and used its in-house solver to perform numerical calculations. Additional functionalities have been added to the solver to model reinforcements. The reinforcements are generally modeled using one-dimensional elements which are incorporated inside a volume model of rubber. In this work, truss elements are formulated to model reinforcements. Primarily, two models have been implemented, namely, the coupled model which models rubber and reinforcements separately with a spring constraint on their displacements to couple them together and an embedded model which involves adding the stiffness contribution of the 1D model to the 3D model. Other simplified models have also been considered.

The effect of the neutral angle, at which the reinforced hose does not deform axially under an internal pressure, has been captured by all the models with the coupled and embedded models having a good agreement with the theoretical value. Further, bending and torsion experiments are simulated using the coupled model. The results of these simulations shows that the model is able to demonstrate the stiffening effect of reinforced hoses and that there is a dependency between pressure and the stiffness of the hose.

Keywords: Hydraulic Hose, Reinforcements, Spring Coupling, Truss Elements, Embedded Technique

Acknowledgement

First, I would like to show my sincere gratitude to my supervisors Christoffer Cromvik and Fredrik Andersson for their guidance, patience and immense knowledge throughout the thesis. Both of them have never hesitated to help me whenever I had doubts and the discussions with them have been useful to get a deeper understanding in this field.

I would also like to thank Fredrik Edelvik at Fraunhofer-Chalmers Centre for giving me the opportunity to work at FCC as a summer intern which paved way for me to do my thesis here.

I thank my examiner Fredrik Larsson for his valuable and timely feedbacks on different issues during the course of this thesis.

I thank Specma AB for giving a tour of their facilities. The visit gave me a practical aspect and relevance of the thesis.

Finally, I would like to thank my family and friends, who have been a constant source of support in whatever I do.

Nomenclature

English Letters

Symbol	Description
a, A	Cross sectional area of a truss element in current and original configuration
\mathbf{a}	Nodal displacements
A_{inner}	Inner surface area of a rubber hose
A_{end}	Cross sectional area of a rubber hose
\mathbf{B}	Strain displacement matrix
\mathbf{C}	Orientation matrix
dl, dL	Length along the truss axis in the current and original configuration
dF	Change in force in three point bending simulation
dw	Change in displacement in three point bending simulation
\mathbf{D}	Constitutive matrix
e	Intersected Elements
E	Young's modulus
f	Force acting on each node in a beam model
f_b	Boundary function
\mathbf{f}	Residual force contribution
F, F_{end}	Forces in a beam model
F_L, F_H	Forces in a hose
\mathbf{F}	Force vector
g	Local coordinate of a truss element
I	Moment of inertia
\mathbf{J}	Jacobian matrix
\mathbf{k}	Stiffness matrix contributions
\mathbf{K}	Stiffness matrix
l, m, n	Direction cosines
L	Length of a hose
n_r	Number of revolutions in a helix
n_{iter}	Number of iterations required in mesh intersection algorithm
n_{nodes}	Number of nodes in a beam model
N	Interpolation function
p	Pressure
P	Pitch of a helix
q, q_{new}	Point used in in MeSomics transformation

Symbol	Description
\mathbf{Q}	Used in truss formulation, $\mathbf{x}_2 - \mathbf{x}_1$
r	Helix radius
\mathbf{r}	Residual
R_i, R_o	Inner and Outer radius of a rubber hose
R_c	Radius of curvature
R_x	Rotational matrix about x coordinate
s	Coordinate along a parametric curve
\mathbf{s}	Helix curve vector
t	Coordinate along a helical curve
t_h	thickness of a rubber hose
T	Truss force
\mathbf{T}	Tangent of a helix
\mathbf{u}	Displacement vector
v_x, v_y, v_z	Components of a vector
w_i	Weights in Gauss quadrature
W	Virtual Work
x, y, z	Coordinate positions of a FE model
\mathbf{x}	Positional vector

Greek Letters

Symbol	Description
θ	Helix angle
θ_R	Angle of resultant force
θ_N	Neutral angle
α	Angle of rotation
δ	Variation of a quantity
ρ	Volume fraction
ν	Poisson's ratio
ϵ	Strain
σ_θ	Hoop stress
σ	Cauchy stress in a truss element
$\epsilon_c, \epsilon_b, \epsilon$	Tolerances in mesh intersection algorithm
ξ, η, τ	Local coordinates of a element
$\boldsymbol{\xi}$	Local coordinate vector
λ	Stretch ratio
κ	Spring constant
π	Mathematical constant

Superscripts

Symbol	Description
e	Element quantity
k	Iterations

Subscripts

Symbol	Description
$1, \dots, 8$	Referring to nodes
e	Element contributions
E	External contributions
i, j, k	Referring to nodes
I	Internal contributions
m	Matrix material
r	Reinforcement
T	Nodes of truss elements
V	Nodes of volume element

Symbols

Symbol	Description
\in	Belonging to
\mathbb{R}	Real number space
\otimes	Outer product

Contents

Abstract	i
Acknowledgement	iii
Nomenclature	v
1 Introduction	1
1.1 Purpose	2
1.2 Goals	3
1.3 Limitations	3
2 Theory	4
2.1 Helical Reinforcements	4
2.1.1 Equations	4
2.1.2 Helix Angle	5
2.1.3 Neutral Angle	5
2.2 Behaviour of Reinforced Hose	6
2.3 Modeling of Reinforcement	7
2.3.1 Smearred model	8
2.3.2 Discrete model	8
2.3.3 Embedded model	8
2.3.4 Coupling 1D elements and 3D elements	9
2.3.5 Modelling as a Composite	10
2.3.6 Other Approaches	10
3 Methodology	11
3.1 Implementation	11
3.1.1 User Element Assembly	12
3.1.2 User Provided General Forces	12
3.2 Beam Model of Reinforcement	13
3.2.1 Beam Element	13
3.2.2 FE Model - Neutral Angle Simulations	13
3.3 Truss Model of Reinforcement	14
3.3.1 Truss Element	14
3.3.2 Formulation	15
3.3.2.1 First Variation of Strain	16
3.3.2.2 Variation of Forces	17
3.3.3 FE Model - Neutral Angle Simulations	18

3.4	Volume Model of Reinforced Hose	18
3.4.1	Hexahedron Element	18
3.4.2	FE Model - Neutral Angle Simulations	21
3.5	Coupled Model	23
3.6	Embedded Model	25
3.6.1	Mesh Intersection Algorithm	26
3.6.1.1	Inverse Mapping	26
3.6.1.2	Boundary Function	27
3.6.1.3	Bisection Method	27
3.6.2	Stiffness contribution of Reinforcement	29
3.7	Abaqus Model	31
3.7.1	FE Model - Neutral Angle Simulations	31
3.8	Bending Simulation	32
3.8.1	Three Point Bending Setup	32
3.8.2	MeSOMICS Setup	33
3.9	Torsion Simulation	35
4	Results & Discussions	36
4.1	Beam Model - Neutral Angle Simulations	36
4.2	Truss Model - Neutral Angle Simulations	38
4.3	Volume Model - Neutral Angle Simulations	39
4.4	Coupled Model - Neutral Angle Simulations	40
4.5	Embedded Model - Neutral Angle Simulations	45
4.6	Abaqus Model - Neutral Angle Simulations	47
4.7	Bending Simulation	47
4.7.1	Three Point Bending	47
4.7.2	MeSOMICS	52
4.8	Torsion Simulation	54
5	Conclusions & Future Work	56
5.1	Conclusions	56
5.2	Future Work	57

List of Figures

1.1	Hydraulic hose with : a) Helically wounded wires and b) Braided reinforcement.	1
1.2	Illustration of three point bending setup.	2
1.3	Results from bending experiments by Specma.	2
2.1	Representation of forces acting in a hose.	6
2.2	Schematic of discrete and embedded model.	9
3.1	Schematic of the implementation with interfaces to the solver.	12
3.2	Beam Element.	13
3.3	FE model of helical steel wire.	13
3.4	Kinematics of a truss element.	15
3.5	Linear Hexahedron Element.	19
3.6	Volume model of a rubber hose.	21
3.7	Helical volume model of a rubber hose.	22
3.8	Row of elements in the default mesh.	22
3.9	Row of elements after transformation.	23
3.10	Schematic of a reinforcement node within a volume element.	24
3.11	Imaginary spring connecting the truss node and the volume node.	24
3.12	FE setup with truss model inside the volume model.	25
3.13	Boundary Function for a Quadratic element.	27
3.14	Intersection determination using Bisection method.	28
3.15	Abaqus model of a) Rubber Hose b) Reinforcement.	31
3.16	Assembly of Rubber Hose and Reinforcement.	32
3.17	Three point bending FE model.	32
3.18	Experimental Setup.	33
3.19	Transformation to form a curved model. a) A point on the straight model. b) The same point on the curved model.	34
3.20	MeSomics FE Model. a) Setup 1: Constrained pressurization. b) Setup 2: Unconstrained pressurization during pressurization step. c) Setup 2: Unconstrained pressurization during displacement steps.	34
3.21	Torsion FE Model.	35
4.1	Beam model setup and deformation.	36
4.2	Results of beam model for 1 bar pressure.	37
4.3	Results of beam model for varying pressures.	38
4.4	Comparison between truss and beam model.	38
4.5	Results of beam model for varying pressures.	39

4.6	Strain contours of volume model.	40
4.7	Results of coupled model for different κ values.	40
4.8	Coupled model deformation in neutral angle simulations. a) Model setup with reinforcements in one direction, b) Model setup with reinforcements in two directions, c) Displacement for reinforcements in one direction, d) Displacement for reinforcements in two directions, e) Strain in the rubber model with reinforcements in one direction, f) Strain in the rubber model with reinforcements in two directions.	41
4.9	Results of coupled model for 1 bar pressure with reinforcement in one direction.	42
4.10	Results of coupled model for 1 bar pressure with reinforcement in two directions.	42
4.11	Mesh convergence study of the coupled model for 1 bar pressure.	43
4.12	Results of coupled model with reinforcement in one direction for varying pressures.	43
4.13	Results of coupled model using different geometries.	44
4.14	Mesh intersecting points.	45
4.15	Strain contours of embedded model.	45
4.16	Results of embedded model for 1 bar pressure.	46
4.17	Results of embedded model with different geometry.	46
4.18	Comparison between Abaqus and Coupled models.	47
4.19	Three point bending model setup and deformation. a) Model setup, b) Deformation with displacement magnitude after pressurization step, c) Deformation with displacement magnitude after displacement steps.	48
4.20	Results from three point bending simulations for varying pressures.	49
4.21	Strain contours on the cross section after pressurization step.	49
4.22	Comparison of bending stiffness.	50
4.23	Results from three point bending simulations for reinforced hose model.	50
4.24	Comparison of bending stiffness vs pressure for different models.	51
4.25	Bending model setup and deformation. a) Model setup 1: constrained pressurization , b) Model setup 2: unconstrained pressurization, c) Deformation with displacement magnitude after pressurization step for setup 1, d) Deformation with displacement magnitude after pressurization step for setup 2, e) Deformation with displacement magnitude after displacement steps for setup 1, f) Deformation with displacement magnitude after displacement steps for setup 2.	52
4.26	Results from Bending Simulations (Setup 1: constrained pressurization).	53
4.27	Results from Bending Simulations (Setup 2: unconstrained pressurization).	53
4.28	Torsion model deformation.	54
4.29	Results from Torsion Simulations.	54
4.30	Results from Torsion Simulations for higher pressures.	55

1

Introduction

Hydraulic hoses are used in industrial applications to transmit fluid at high pressure. The hoses are designed to withstand high pressure and at the same time be flexible in order to meet machine operation and maintenance requirements. Usually, a high-pressure hose consists of interior and exterior layers of rubber complemented with a number of layers of steel wire and rubber in between. The inner rubber layer is placed to resist leakage and chemical damage, and the outer rubber layer is designed for abrasion resistance. There are two types of reinforcing steel layers: helically wounded wires (spiral hose) and braids as represented in Figure (1.1). For a spiral hose, it is common to have an even number of helices and alternate between left and right. The helix or braid angle, defined as the angle between the tangent of a steel wire and the hose axis, is usually chosen to minimize the change in hose length and to avoid torsion when the hose is pressurized.



a)



b)

Figure 1.1: Hydraulic hose with : a) Helically wounded wires and b) Braided reinforcement.

Specma AB, which is a manufacturer and a supplier of hydraulics, performs various tests on the hoses before it is approved for industrial usage. They are subjected to a pressure range of 0 to 400 bars within a second which is repeated for two hundred thousand cycles. It is essential for them to understand how a reinforced hose behaves in order to improve its performance.

1.1 Purpose

Fraunhofer Chalmers Centre (FCC) has an ongoing cooperation with Specma AB and Fraunhofer ITWM on simulation of pressurized hoses. The main focus until now has been on rapid simulations of hose deformation at low pressures. Measurements of bending stiffness at different pressure levels have been performed using a three point bending rig and a finite element (FE) rod model has been developed and validated for isotropic hoses. Three point bending is a traditional method to study the bending stiffness of a rubber hose. The rubber hose is rested on two supports and is subjected to a load at its centre. The illustration of the experimental setup is presented in Figure (1.2).

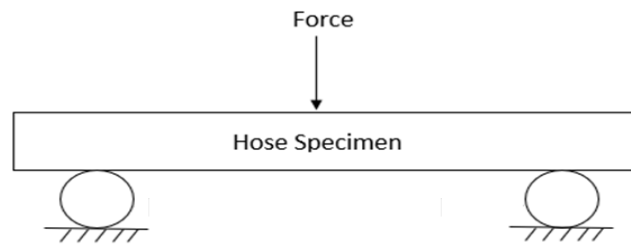


Figure 1.2: Illustration of three point bending setup.

Application of the same model to steel reinforced hoses has seen less success. The reinforced hose shows considerable stiffening when pressurized as shown in Figure (1.3). The steel reinforcement is stiff, but only as long as external forces are balanced by the tensile forces in the wires. With internal pressure, the wires are subjected to tension and can sustain the state of tension during bending of the hose. The pressure can also cause wire interaction such that the reinforcements interlocks, which causes further increased stiffness.

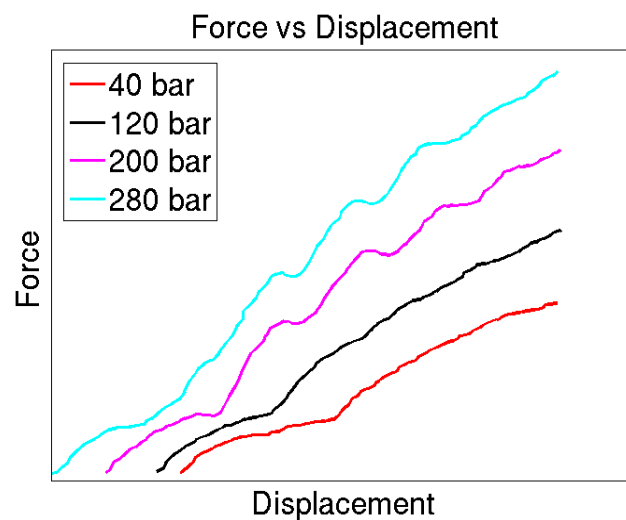


Figure 1.3: Results from bending experiments by Specma.

Thus, there is long-term project at FCC to investigate the cause of the increased stiffness for the reinforced hose and to construct a computational model to demonstrate the stiffening behaviour, for which this thesis would serve as a starting point. The main aim of the thesis is to model the reinforcements effectively.

1.2 Goals

The goals of the master's thesis are given below:

- To select and implement a suitable model or models from literature that can effectively predict the behaviour of reinforcements.
- To study the effect of different helix angles under pressurization.
- To compare the results with published results and analytical expressions.
- To study the behaviour of the model in bending and in torsion.

1.3 Limitations

The thesis focused on modeling of helical reinforcements and braided reinforcements are not considered. Further, the contact between multiple reinforcements will be ignored to simplify the problem at hand. The thesis does not aim to model the reinforced hose with multiple layers which were used in the experiments performed by Specma. Thus, for bending and torsion simulations, the results of the simulations cannot be compared with experimental results.

2

Theory

Analytical explanations of physical phenomenon are generally termed as mathematical modeling [1]. Mathematical models are derived from the physics of the problem using suitable governing equations and underlying assumptions. These models are commonly solved using numerical methods. The finite element method is one such numerical method which is used to solve differential equations in the field of engineering. Analysis of structures, heat transfer and fluid problems are some examples in which the finite element method is applied. The method involves discretization of a geometric domain into a number of sub domains or finite elements. The properties of each element is determined separately depending on the geometry and the equations used. All the element equations are assembled based on the discretization and are solved to determine the unknown quantity.

The theory behind modeling of rubber hoses and reinforcements from the literature are explained in this chapter.

2.1 Helical Reinforcements

2.1.1 Equations

The parametric equations of a helix curve [2] are,

$$\begin{aligned}x(t) &= r \cdot \cos(t), \\y(t) &= r \cdot \sin(t), \\z(t) &= b \cdot t,\end{aligned}\tag{2.1}$$

for $t \in [0, 2\pi]$ where r is the radius of the helix and b is a constant related to the pitch of the helix. The pitch P , is defined as the the distance along the z axis of one complete revolution of a helix,

$$P = \frac{2\pi r}{\tan \theta} = 2\pi b,\tag{2.2}$$

where θ is called the helix angle. If the helix curve is represented as $\mathbf{s}(t)$ ($\mathbf{s}(t) = [x(t), y(t), z(t)]$), the normalized tangent of the helix is defined as,

$$\mathbf{T}(t) = \frac{\mathbf{s}'(t)}{\|\mathbf{s}'(t)\|}. \quad (2.3)$$

2.1.2 Helix Angle

The helix angle or the braid angle is defined as the angle between the tangent to the helix and the axial direction of the hose. The effects of the helix angle in a hydraulic hose has been extensively studied in several papers [3–5]. The helix angle plays an important role in determining the behaviour of the hose and its overall life.

2.1.3 Neutral Angle

Particularly, scholars have studied the neutral angle [3], at which, there is no deformation of the hose when pressurized. At any angle other than the helix angle, the braid or the helix moves in the direction which would make the helix angle equal to the neutral angle so as to counter the internal forces. Thus, when the helix angle is greater than the neutral angle, the hose extends in length with a decrease in its diameter and when the helix angle is lesser than the neutral angle, the hose will contract in length with increase in diameter.

Let a straight hollow cylinder with inner radius R_i , outer radius R_o , and thickness t_h , represent the hose which is subjected to an internal pressure p . Now, consider a segment of the cylinder with length L . Due to the internal pressure, the segment is subjected to a longitudinal force F_L and a circumferential force F_H . The longitudinal force can be defined as,

$$F_L = p\pi R_i^2. \quad (2.4)$$

The circumferential force balances the hoop stress, σ_θ . Assuming thin-walled cylinder conditions (the thickness of the cylinder should not be more than one-tenth of its mean radius), σ_θ acting on the hose and F_H are given by,

$$\begin{aligned} \sigma_\theta &= \frac{pR_i}{t_h}, \\ F_H &= \sigma_\theta t_h L = \frac{pR_i}{t_h} t_h L = pR_i L. \end{aligned} \quad (2.5)$$

The angle of the resultant force, θ_R due to the internal pressure,

$$\tan \theta_R = \frac{F_H}{F_L} = \frac{L}{\pi R_i}. \quad (2.6)$$

The forces acting on a reinforced hose are presented in Figure (2.1).

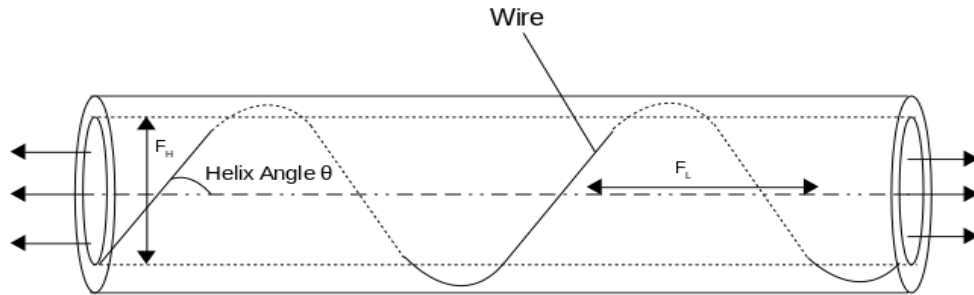


Figure 2.1: Representation of forces acting in a hose.

For equilibrium to exist, the helix angle should be aligned to the angle of the resultant force due to the internal pressure. Thus, $\theta = \theta_R$.

From the geometry of helix,

$$L = \frac{2\pi R_i}{\tan \theta}. \quad (2.7)$$

Thus, combining Equation (2.6) and Equation (2.7),

$$\begin{aligned} \tan \theta_R &= \tan \theta = \frac{2}{\tan \theta}, \\ \tan^2 \theta &= 2, \\ \theta &\approx 54.74. \end{aligned} \quad (2.8)$$

This is the neutral angle, $\theta_N = \theta$, at which there should be no deformation of the hose when pressurized.

2.2 Behaviour of Reinforced Hose

Entwistle and White [5, 6] have studied extensively the behaviour of hydraulic hoses reinforced by braided layers and steel wires. Specifically, they have stated a method to calculate the elastic strains in the wires and the change in length of the hose analytically for a pressurized hydraulic hose with two layers of reinforcements. The analytical method has been compared with experimental values and has been found to have good agreement. In order to transfer the load between the inner and outer layer effectively, it is recommended that the reinforcements are laid down at helix angles which vary symmetrically about the neutral angle. If the angles lie asymmetrically, the inner layer is subjected to a high tension compared to the outer layer. Thus, the inner layer would reach the fatigue limit earlier causing the hose to fail at

pressure values less than expected ones. It is recommended that the difference between the helix angles of the inner and outer layer should vary by a minimum of 4° to produce load sharing contact between the reinforcement layers. With increase in the angle difference, it is found that the ratio of tensions between inner and outer layers increase.

Hydraulic hose failures have been studied in detail by the HF subcommittee Society of Automotive Engineers(SAE) [3]. In contrast to the theoretical neutral angle, in reality, the equilibrium does not always occur at 54.74° . According to SAE standards, a 2% increase or a 4% decrease in hose length is said to be within allowable limits when the hose is pressurized. It is because of the fact that most of the reinforcing materials have some degree of stretch under stress which cannot be controlled precisely. Moreover, it should not be assumed that the reinforcements takes up the entire load. The rubber layer in between the reinforcement layers does sustain a portion of the internal load.

There have been other numerical approaches to characterize the behaviour of high pressure reinforced hoses. Van der Hoon et al [4] considered a straight tube with a single braid layer and have calculated stress and strains due to internal pressure for small deformations using a membrane model with elastic steel fibres, a membrane model with inextensible wires and a thick walled tube model. As a continuation, an approximate analysis of the stresses and strains in a spiral hose have been given by P.C Bregman et al [7].

Further, by using a continuum approach, analytical solutions for bending and flexure of helically reinforced cylinder under a uniform load is described by J.A Crossly et al [8]. Each layer of the cylinder is assumed to be transversely isotropic, whose principal direction is along a helix surrounding the central axis of the cylinder. Also, a flexible pipe has been regarded as a laminated structure by GU Fan et al [9] consisting of multiple anisotropic reinforcement layers and multiple isotropic rubber layers. By using three-dimensional (3D) anisotropic elastic theory, analytical solutions have been presented for displacement distribution, strain distribution and stress distribution. In this analysis, the flexible pipe is assumed to be infinite and thus the method is applicable for pipe away from the ends.

2.3 Modeling of Reinforcement

Reinforcements modeling have been more often employed to model reinforcements in reinforced concrete. Similar modeling techniques can be used to model helical reinforcements in an hydraulic hose by considering rubber as the matrix and steel wires as reinforcements. Commonly, the matrix material is modeled using solid or volume elements and the reinforcements are modeled using beam or truss elements. There are several models available in literature to link the reinforcements with the matrix. The predominant models are

- Smearred model [10, 11],
- Discrete model [10, 12],
- Embedded model [10, 12, 13].

2.3.1 Smearred model

In the smeared model [10, 11], the reinforcements are considered to be smeared over the volume elements of the matrix. The constitutive tensor \mathbf{D} , which relates stress $\boldsymbol{\sigma}$, and strain $\boldsymbol{\epsilon}$, ($\boldsymbol{\sigma} = \mathbf{D}\boldsymbol{\epsilon}$) for an element is derived as the weighted sum of the constitutive tensor of the matrix material and the reinforcement,

$$\mathbf{D} = \rho_m \mathbf{D}_m + \rho_r \mathbf{D}_r, \quad (2.9)$$

where \mathbf{D}_m and \mathbf{D}_r refer to the constitutive tensor of the matrix and the reinforcement respectively with ρ_m and ρ_r referring to the volume ratios of the matrix and the reinforcement in an element. In three-dimensional cases, the size of \mathbf{D} , \mathbf{D}_m and \mathbf{D}_r matrices would be 6 x 6.

The reinforcement is assumed to contribute only in its longitudinal direction. The smeared approach is said to be a good model for modeling distributed reinforcements and is able to reproduce the overall behaviour of the structure. But, the model suffers from local stress concentrations which may result in mesh dependency and non-physical results [13].

2.3.2 Discrete model

In the discrete model [10, 12], one-dimensional (1D) elements are added along the edges of the volume elements. These elements are considered as a spring between two nodes of the mesh. The global stiffness matrix is modified in this case,

$$\mathbf{K} = \mathbf{K}_m + \sum_{i=1}^{N_r} \mathbf{K}_{r,i}, \quad (2.10)$$

where \mathbf{K}_m is the global stiffness matrix of the volume elements and $\mathbf{K}_{r,i}$ is the stiffness matrix of i^{th} reinforcement with N_r being the total number of reinforcements.

The model has a better representation of the reinforcements when compared with the smeared model, thus allowing for a more accurate behaviour. But the major disadvantage of the model is that the mesh of the solid elements should follow that of the 1D elements or vice versa so that the nodes are shared by both the meshes. While this approach may be good for modelling in some cases, it would become difficult if there are many reinforcement layers to be modeled.

2.3.3 Embedded model

The embedded model is a more generalized approach of the discrete model [10, 12, 13]. This model allows for any reinforcement layout irrespective of the volume mesh. It allows for reinforcements to go through the volume elements. The element stiffness matrix is modified in this model as,

$$\mathbf{K}_e = \mathbf{K}_{m,e} + \sum_{i=1}^{N_r} \mathbf{K}_{r,i,e}, \quad (2.11)$$

where N_r represents the number of reinforcements crossing an element of the volume mesh and e denotes that the matrix is a element matrix.

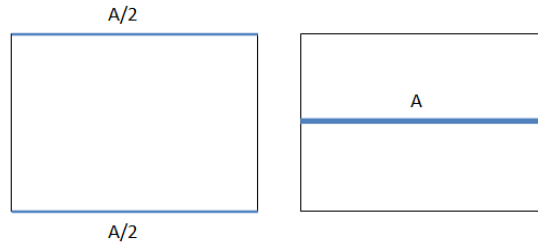


Figure 2.2: Schematic of discrete and embedded model.

It is recommended to have a fine mesh of the solid elements at the ends or at any places where there might be a stress singularity due to geometric discontinuities [13]. The difference between the discrete and the embedded approach can be visualized in Figure (2.2). The element on the left has reinforcement along the nodes of the volume element whereas the element on the right has the reinforcement going through the element. The embedded approach is more flexible with respect to mesh constraints compared to the discrete model.

2.3.4 Coupling 1D elements and 3D elements

To perform multi-dimensional coupling, it is essential to enforce constraints on the models to be coupled such that the displacements are compatible at the interface [14]. Dermot et al have derived multipoint constraints to equate the axial force, bending moment, shear force and torsion to couple 1D beams to 3D elements.

For application in reinforced geometrical structures, Sadek et al [15] formulated a 3D embedded beam element. The 3D embedded beam element considers a beam element within a solid element. The translation degrees of freedom for the beam element are removed and are written in terms of interpolated values of the solid element. Turello et al [16] improved the embedded beam element with the introduction of interaction surface. The embedded element has been found to be useful for applications involving beam elements interacting with solid elements. Further, Ninic et al [17] proposed a contact formulation for the embedded element with arbitrary orientation. Interaction conditions have been enforced in the integration points of the beam elements which are projected to respective control points of the respective volume elements.

2.3.5 Modelling as a Composite

Commonly, hydraulic hoses are modelled as a rubber/steel wire composite laminated structure. Breig [18] have performed an analysis of a spiral hose using laminate theory and the results have shown good correspondence with Entwistle's analytical solution for change in helix angle with change in length when subjected to pressure. In a more recent work by J.R.Cho et al [19], homogenization techniques have been implemented to determine the orthotropic material properties of the reinforcement layer which has been used as inputs for simulating the torsional behaviour of a rubber hose.

The homogenization procedure involves defining a representative volume element (RVE). A representative volume element is generally considered as a small volume which is capable of representing the behaviour of the overall composite material. In [19], a RVE of a braided fabric is defined and using the superposition method, a number of unit cell finite analyses is performed from which the homogenized material properties are determined. The homogenized orthotropic model of the rubber hose has been found to capture its behaviour in torsion better when compared to a homogenized isotropic model.

2.3.6 Other Approaches

There have been many other approaches which has been recently developed to model reinforcements. One such method is the mixed dimensional modelling method which has been proposed by Benoit et al [11]. It allows to have a 3D representation of the reinforcements in zones of interest and a 1D representation in the rest of the structure. The concept of the eXtended finite element method has been used to model the linkage between 1D and 3D elements. Another approach by Llau et al [13], called "1D-3D", generates an equivalent volume from a 1D mesh of the reinforcements. The associated stiffness and stresses are condensed on the boundary of the newly generated volume that are applied to the 3D elements using kinematic coupling.

Based on the literature survey, the reinforcements and the rubber hose will be modeled using one-dimensional and three-dimensional elements respectively. Further, an embedded model and a coupled model are chosen to be the primary focus of the work since these models can be easily extended to model interactions between the reinforcements.

3

Methodology

Three different simulation studies have been performed in this work. Initially, to study the effect of the neutral angle, the helix angle has been varied and the change in length for each angle has been determined. These simulations will be referred to as neutral angle simulations. Further, bending and torsion studies have been conducted with the reinforcement models. The reinforcements are modeled using one-dimensional elements and the rubber hose is modeled using three-dimensional elements. A three-dimensional space is considered in x, y, z directions. The element formulations, models and the methodologies used are explained in this chapter. Models of reinforcements alone are considered at first without the rubber hose and later, the whole rubber hose with reinforcements are modeled. Young's modulus of 200 GPa has been used for steel and 10 MPa has been used for rubber. A Poisson's ratio of 0.3 is used for rubber since there is no dependency on Poisson's ratio and values closer to 0.5 causes convergence issues due to volumetric locking.

3.1 Implementation

The thesis uses FCC's in-house finite element software for structural statics and dynamics, LaStFEM. The software includes a wide variety of material models for metals and polymers and allows analysis of beams, shells and volumes subject to large deformations and mechanical contacts [20]. Emphasis is on multi-physics applications such as thermo-mechanical simulations of welding and fluid-structure interactions. LaStFEM uses a total Lagrangian formulation to solve problems with both geometric and material non-linearities. The formulation is in terms of the Lagrangian measures of stress and strain in which the derivatives and integrals are taken with respect to the Lagrangian coordinates. In the Lagrangian approach, the nodes and elements move with the material. The constitutive equations will always be evaluated at the same material point. The formulation and the implementation of the method is based on the description in [21]. LaStFEM has been used in welding applications [22–27], in fluid-structure interactions [28, 29] and in simulation of composites [30, 31]. In each time step, LaStFEM finds a solution x which solves the balance of internal forces, \mathbf{F}_I and external forces, \mathbf{F}_E such that $\mathbf{F}_I + \mathbf{F}_E = 0$.

A block diagram representing the implementation part in the thesis is shown in Figure (3.1). The case setups, including node, element and load definitions are scripted in Lua which would call the built-in functions of LaStFEM. Further, to add elements which are not present in LaStFEM or to include additional

forces to the model, two interfaces exist to the solver which are briefly explained here.

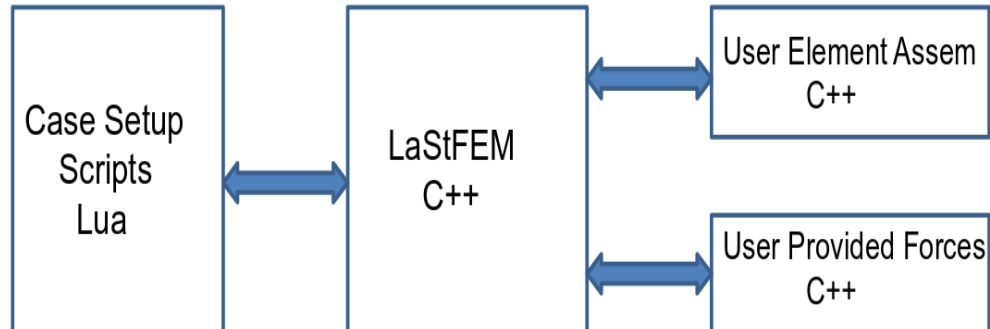


Figure 3.1: Schematic of the implementation with interfaces to the solver.

3.1.1 User Element Assembly

The purpose of the function is to compute the contribution of internal forces and stiffness for the user defined elements. In the thesis, truss elements are formulated as user-defined elements. The elements and corresponding nodes are created in the setup. The nodal positions and displacements of the element is available as inputs to this function. Further, it is also possible to pass arbitrary values as user parameters. For each element, this function would calculate and return the internal force vector and corresponding stiffness matrix which would be assembled in the global matrix. The calculations from the truss formulation described in Section 3.3.2 would be performed in this function.

3.1.2 User Provided General Forces

To couple different models together, it is necessary to define constraints on them. This can be enforced with a penalty formulation. A spring constraint is introduced as explained in Section 3.5. The spring force is added to the external forces and the stiffness contribution is added to the global stiffness matrix. The residual force and stiffness contributions from the spring formulation would be performed in this function. The nodal positions and displacements of the whole model would be available as inputs and it also possible to pass user parameters to this function as well.

3.2 Beam Model of Reinforcement

3.2.1 Beam Element

LaStFEM has the ability to handle beam elements. Thus, the reinforcements are initially modeled using beam elements. A beam element is a slender structural member capable of handling axial and shear forces along with bending and torsional moments. Beam elements can be formulated in two or three-dimensional spaces. Three-dimensional beam elements with two nodes are considered for modeling reinforcements in this section. Each node has three translational degrees of freedom and three rotational degrees of freedom. Beam elements are commonly used to model components which has its length much higher than other dimensions. A beam element with two nodes is presented in Figure (3.2).

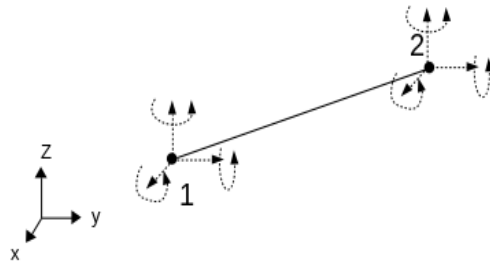


Figure 3.2: Beam Element.

3.2.2 FE Model - Neutral Angle Simulations

To study the effect of the neutral angle, the reinforcements alone are modeled using beam elements. The FE model is shown in Figure (3.3).



Figure 3.3: FE model of helical steel wire.

The model is generated by using Equation (2.1) with a radius of 10 mm and having 3 revolutions. A routine is developed which would generate the mesh of the helical reinforcement based on the input values of radius, helix angle and number of revolutions. The internal pressure is converted into a force on each node. The sum of the forces in all the nodes of the reinforcement should be equal to force F , generated by internal pressure p , in the circumferential direction,

$$\begin{aligned} F &= p \cdot A_{inner} = pL2\pi r = n_{nodes}f_i, \\ f_i &= \frac{pL2\pi r}{n_{nodes}}, \end{aligned} \quad (3.1)$$

where n_{nodes} is the number of nodes in the model, A_{inner} is the inner area subjected to pressure, r is radius of the helix, L is the length of the model and f_i is the force acting on each node. To account for end forces, a load is set in the end node equivalent to the force acting on the end caps in axial direction,

$$F_{end} = p \cdot A_{end} = p\pi r^2. \quad (3.2)$$

The reinforcement is fully constrained at the left end and at the right end it is free to move only in axial direction. The rotational degrees of freedom are constrained at both ends.

3.3 Truss Model of Reinforcement

3.3.1 Truss Element

Truss elements are one-dimensional elements which are capable of transmitting axial force. Truss elements are commonly used for structures which are long compared to its cross sections. They are assumed to have a constant cross section with three translational degrees of freedoms at each node. The truss elements differ from beam elements in that beam elements has the capability to sustain bending moments and shear forces along with tension and compressive forces whereas truss elements are capable in handling tension and compressive forces alone. Since the reinforcements are considered to have stiffness only in their longitudinal direction, truss elements with two nodes are a good choice to model the reinforcements and faster to assemble with fewer degrees of freedom. Also, in case of coupling with 3D elements, truss elements are easily compatible since truss and 3D elements have the same degrees of freedom for each node.

A typical truss structure is shown in Figure (3.4). The element has nodes 1 and 2 whose current position is denoted as $\mathbf{x}_1 \in \mathbb{R}^3$ and $\mathbf{x}_2 \in \mathbb{R}^3$. The displacements of the nodes are given as $\mathbf{u}_1 \in \mathbb{R}^3$ and $\mathbf{u}_2 \in \mathbb{R}^3$. A parametric coordinate g , is defined along the element with $-1 \leq g \leq 1$ with one node at $g = -1$ and another at $g = 1$. The Abaqus theory manual [32] has been used as a starting point in the formulation described in following subsection.

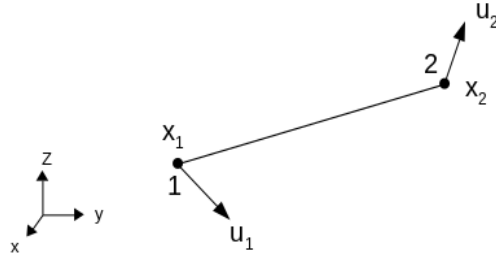


Figure 3.4: Kinematics of a truss element.

3.3.2 Formulation

LaStFEM does not have the capability to handle truss elements at present. The internal force and stiffness contributions for a truss element should be formulated to be able to integrate them with LaStFEM. The interpolation functions for the two node truss element are given as,

$$\begin{aligned} N_1 &= \frac{1}{2}(1 - g), \\ N_2 &= \frac{1}{2}(1 + g). \end{aligned} \tag{3.3}$$

Using the interpolation functions, the displacements and positions along the element can be interpolated as,

$$\begin{aligned} \mathbf{u}(g) &= N_1 \mathbf{u}_1 + N_2 \mathbf{u}_2, \\ \mathbf{x}(g) &= N_1 \mathbf{x}_1 + N_2 \mathbf{x}_2. \end{aligned} \tag{3.4}$$

The current position of the nodes is given by,

$$\begin{aligned} \mathbf{x}_1 &= \mathbf{X}_1 + \mathbf{u}_1, \\ \mathbf{x}_2 &= \mathbf{X}_2 + \mathbf{u}_2, \end{aligned} \tag{3.5}$$

where \mathbf{X}_1 and \mathbf{X}_2 are the original undeformed positions of the two nodes.

The stretch ratio along the axis is,

$$\lambda = \frac{dl}{dL}, \tag{3.6}$$

where dl measures the length along the truss axis in the current configuration,

$$dl = \sqrt{\frac{d\mathbf{x}}{dg} \cdot \frac{d\mathbf{x}}{dg}} dg, \tag{3.7}$$

and dL measures the length along the truss axis in the original configuration.

For a geometrically non-linear analysis, a logarithmic strain is considered,

$$\epsilon = \ln\left(\frac{dl}{dL}\right). \quad (3.8)$$

From Equation (3.4), the term $\frac{d\mathbf{x}}{dg}$ can be written as,

$$\frac{d\mathbf{x}}{dg} = \frac{dN_1}{dg} \mathbf{x}_1 + \frac{dN_2}{dg} \mathbf{x}_2 = \frac{\mathbf{x}_2 - \mathbf{x}_1}{2}. \quad (3.9)$$

Therefore, the stretch ratio can be determined as,

$$\lambda = \frac{dl}{dL} = \sqrt{\frac{d\mathbf{x}}{dg} \cdot \frac{d\mathbf{x}}{dg} \frac{dg}{dL}} = \frac{|\mathbf{x}_2 - \mathbf{x}_1|}{L}, \quad (3.10)$$

where L is the initial length.

3.3.2.1 First Variation of Strain

The first variation of strain is,

$$\delta\epsilon = \frac{1}{\left(\frac{dl}{dL}\right)} \delta\left(\frac{dl}{dL}\right). \quad (3.11)$$

Using the relation in Equation (3.10),

$$\begin{aligned} \delta\left(\frac{dl}{dL}\right) &= \frac{dg}{dL} \frac{1/2}{\sqrt{\frac{d\mathbf{x}}{dg} \cdot \frac{d\mathbf{x}}{dg}}} \cdot 2 \frac{\mathbf{x}}{dg} \cdot \delta\left(\frac{d\mathbf{x}}{dg}\right), \\ &= \frac{dg}{dL} \frac{dg}{dl} \frac{d\mathbf{x}}{dg} \delta\left(\frac{d\mathbf{x}}{dg}\right), \\ &= \frac{dg}{dL} \mathbf{t} \cdot \delta\left(\frac{d\mathbf{x}}{dg}\right), \end{aligned} \quad (3.12)$$

where $\mathbf{t} = \frac{dg}{dl} \frac{d\mathbf{x}}{dg}$.

Thus,

$$\delta\epsilon = \frac{1}{\left(\frac{dl}{dL}\right)} \frac{dg}{dL} \mathbf{t} \cdot \delta\left(\frac{d\mathbf{x}}{dg}\right) = \frac{dg}{dl} \mathbf{t} \cdot \delta\left(\frac{d\mathbf{x}}{dg}\right). \quad (3.13)$$

Using the relations in Equations (3.7) and (3.9), the terms in the Equation (3.13) are expanded as,

$$\begin{aligned}\frac{dg}{dl} &= \frac{1}{\sqrt{\frac{d\mathbf{x}}{dg} \cdot \frac{d\mathbf{x}}{dg}}} = \frac{2}{|\mathbf{x}_2 - \mathbf{x}_1|}, \\ \left(\frac{d\mathbf{x}}{dg}\right) &= \left(\frac{\mathbf{x}_2 - \mathbf{x}_1}{2}\right), \\ \delta\left(\frac{d\mathbf{x}}{dg}\right) &= \delta\left(\frac{\mathbf{x}_2 - \mathbf{x}_1}{2}\right) = \frac{\delta\mathbf{x}_2 - \delta\mathbf{x}_1}{2}.\end{aligned}\tag{3.14}$$

Finally,

$$\delta\epsilon = \frac{1}{|\mathbf{x}_2 - \mathbf{x}_1|^2}(\mathbf{x}_2 - \mathbf{x}_1)(\delta\mathbf{x}_2 - \delta\mathbf{x}_1).\tag{3.15}$$

The virtual work contribution from stress in a truss element is,

$$\delta W = \int_l a \sigma \delta\epsilon dl,\tag{3.16}$$

where a is the current cross section, l is the current length and σ is the Cauchy's stress. Assuming that the truss element is incompressible, $adl = AdL$, where A and L are the cross section and length in the original configuration. So,

$$\delta W = \int_L A \sigma \delta\epsilon dL.\tag{3.17}$$

Using the relation, $\sigma = E\epsilon$, where E is the Young's Modulus of the material, the virtual work contribution is,

$$\delta W = \int_L AE \epsilon \delta\epsilon dL.\tag{3.18}$$

Thus, the virtual work contribution to the internal force from one truss element is,

$$\begin{aligned}\mathbf{f}_1 &= -LT \frac{1}{|\mathbf{x}_2 - \mathbf{x}_1|^2}(\mathbf{x}_2 - \mathbf{x}_1), \\ \mathbf{f}_2 &= LT \frac{1}{|\mathbf{x}_2 - \mathbf{x}_1|^2}(\mathbf{x}_2 - \mathbf{x}_1),\end{aligned}\tag{3.19}$$

where $T = EA\epsilon$ is the axial force.

3.3.2.2 Variation of Forces

The second variation of strain gives the stiffness matrix. The equivalent can be achieved by the variation of forces in Equation (3.19) with respect to $\mathbf{x}_1, \mathbf{x}_2$. Since \mathbf{f}_1 and \mathbf{f}_2 differ by a negative sign, taking \mathbf{f} to reduce complication as,

$$\mathbf{f} = -LT \frac{1}{|\mathbf{x}_2 - \mathbf{x}_1|^2}(\mathbf{x}_2 - \mathbf{x}_1)\tag{3.20}$$

$$\begin{aligned} \delta \mathbf{f} = & -LT \frac{1}{|\mathbf{x}_2 - \mathbf{x}_1|^2} (\delta \mathbf{x}_2 - \delta \mathbf{x}_1) - LEA \frac{1}{|\mathbf{x}_2 - \mathbf{x}_1|^2} (\mathbf{x}_2 - \mathbf{x}_1) \otimes \delta \epsilon \\ & + LT \frac{1}{|\mathbf{x}_2 - \mathbf{x}_1|^4} 2(\mathbf{x}_2 - \mathbf{x}_1) \otimes (\mathbf{x}_2 - \mathbf{x}_1) (\delta \mathbf{x}_2 - \delta \mathbf{x}_1). \end{aligned} \quad (3.21)$$

The third contribution in the above term is a result of,

$$\begin{aligned} \delta \left(\frac{1}{|\mathbf{x}_2 - \mathbf{x}_1|^2} \right) &= \delta [(\mathbf{x}_2 - \mathbf{x}_1)(\mathbf{x}_2 - \mathbf{x}_1)]^{-1} \\ &= \frac{1}{|\mathbf{x}_2 - \mathbf{x}_1|^4} 2(\mathbf{x}_2 - \mathbf{x}_1) \otimes (\mathbf{x}_2 - \mathbf{x}_1) (\delta \mathbf{x}_2 - \delta \mathbf{x}_1). \end{aligned} \quad (3.22)$$

Using the first variation of strain from Equation (3.15),

$$\delta \mathbf{f} = \mathbf{k}(\delta \mathbf{x}_1 - \delta \mathbf{x}_2), \quad (3.23)$$

with

$$\mathbf{k} = \frac{LT}{|\mathbf{Q}|^2} \mathbf{I} + \frac{LEA}{|\mathbf{Q}|^4} \mathbf{Q}\mathbf{Q}^T - \frac{2LT}{|\mathbf{Q}|^4} \mathbf{Q}\mathbf{Q}^T, \quad (3.24)$$

where $\mathbf{Q} = \mathbf{x}_2 - \mathbf{x}_1$. Thus, the variation of forces are,

$$\begin{bmatrix} \delta \mathbf{f}_1 \\ \delta \mathbf{f}_2 \end{bmatrix} = \mathbf{K} \begin{bmatrix} \delta \mathbf{x}_1 \\ \delta \mathbf{x}_2 \end{bmatrix}, \quad (3.25)$$

where \mathbf{K} is the stiffness matrix which is assembled as,

$$\mathbf{K} = \begin{bmatrix} \mathbf{k} & -\mathbf{k} \\ -\mathbf{k} & \mathbf{k} \end{bmatrix}. \quad (3.26)$$

3.3.3 FE Model - Neutral Angle Simulations

To study the effect of the neutral angle using the truss model, a FE model is setup similar to the beam model as explained in Section 3.2.2.

3.4 Volume Model of Reinforced Hose

3.4.1 Hexahedron Element

Linear hexahedron elements are used to model the reinforced hose. The element has eight nodes located at the corner with three translational degrees of freedom at each node. The element and the node numbering is shown in Figure (3.5). The formulation of a hexahedron element [33] is explained briefly since it will be used later on.

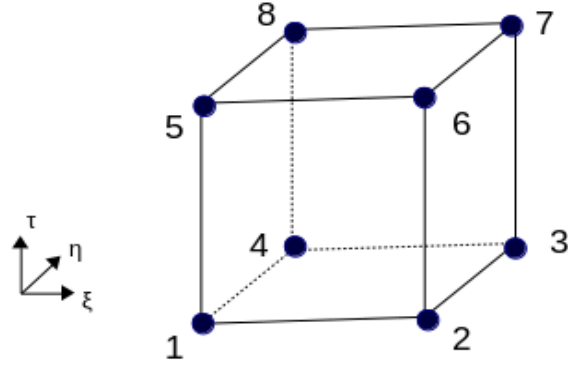


Figure 3.5: Linear Hexahedron Element.

The interpolation or basis functions of the element are given below,

$$\begin{aligned}
 N_1 &= \frac{1}{8}(1 - \xi)(1 - \eta)(1 - \tau), & N_5 &= \frac{1}{8}(1 - \xi)(1 - \eta)(1 + \tau), \\
 N_2 &= \frac{1}{8}(1 + \xi)(1 - \eta)(1 - \tau), & N_6 &= \frac{1}{8}(1 + \xi)(1 - \eta)(1 + \tau), \\
 N_3 &= \frac{1}{8}(1 + \xi)(1 + \eta)(1 - \tau), & N_7 &= \frac{1}{8}(1 + \xi)(1 + \eta)(1 + \tau), \\
 N_4 &= \frac{1}{8}(1 - \xi)(1 + \eta)(1 - \tau), & N_8 &= \frac{1}{8}(1 - \xi)(1 + \eta)(1 + \tau),
 \end{aligned} \tag{3.27}$$

where $\xi \in [-1, 1]$, $\eta \in [-1, 1]$, $\tau \in [-1, 1]$. The interpolated displacement in the element is given by,

$$\begin{bmatrix} u \\ v \\ w \end{bmatrix} = [\mathbf{N}] \begin{bmatrix} u_1 \\ v_1 \\ w_1 \\ u_2 \\ v_2 \\ w_2 \\ \cdot \\ \cdot \\ \cdot \\ w_8 \end{bmatrix} = [\mathbf{N}][\mathbf{a}], \tag{3.28}$$

where \mathbf{a} is the nodal displacement vector, u is the displacement in x direction, v is the displacement in y direction, w is the displacement in z direction and,

$$[\mathbf{N}] = \begin{bmatrix} N_1 & 0 & 0 & \cdot & \cdot & \cdot & N_8 & 0 & 0 \\ 0 & N_1 & 0 & \cdot & \cdot & \cdot & 0 & N_8 & 0 \\ 0 & 0 & N_1 & \cdot & \cdot & \cdot & 0 & 0 & N_8 \end{bmatrix}. \tag{3.29}$$

The strains can be expressed as,

$$[\boldsymbol{\epsilon}] = \begin{bmatrix} \epsilon_{xx} \\ \epsilon_{yy} \\ \epsilon_{zz} \\ \epsilon_{xy} \\ \epsilon_{yz} \\ \epsilon_{zx} \end{bmatrix} = \begin{bmatrix} \frac{\partial u}{\partial x} \\ \frac{\partial v}{\partial y} \\ \frac{\partial w}{\partial z} \\ \frac{1}{2} \frac{\partial u}{\partial y} + \frac{1}{2} \frac{\partial v}{\partial x} \\ \frac{1}{2} \frac{\partial v}{\partial z} + \frac{1}{2} \frac{\partial w}{\partial y} \\ \frac{1}{2} \frac{\partial u}{\partial z} + \frac{1}{2} \frac{\partial w}{\partial x} \end{bmatrix} = [\mathbf{B}][\mathbf{a}], \quad (3.30)$$

where \mathbf{B} is the strain displacement matrix.

$$[\mathbf{B}] = \begin{bmatrix} \mathbf{B}_1 & \mathbf{B}_2 & \dots & \mathbf{B}_8 \end{bmatrix}, \quad (3.31)$$

$$[\mathbf{B}_i] = \begin{bmatrix} \frac{\partial N_i}{\partial x} & 0 & 0 \\ 0 & \frac{\partial N_i}{\partial y} & 0 \\ 0 & 0 & \frac{\partial N_i}{\partial z} \\ \frac{\partial N_i}{\partial y} & \frac{\partial N_i}{\partial x} & 0 \\ 0 & \frac{\partial N_i}{\partial z} & \frac{\partial N_i}{\partial y} \\ \frac{\partial N_i}{\partial z} & 0 & \frac{\partial N_i}{\partial x} \end{bmatrix}, \quad i = 1, \dots, 8.$$

The relationship between the derivatives of the basis functions with respect to local and the global coordinates are given by,

$$\begin{bmatrix} \frac{\partial N_i}{\partial x} \\ \frac{\partial N_i}{\partial y} \\ \frac{\partial N_i}{\partial z} \end{bmatrix} = [\mathbf{J}]^{-1} \begin{bmatrix} \frac{\partial N_i}{\partial \xi} \\ \frac{\partial N_i}{\partial \eta} \\ \frac{\partial N_i}{\partial \tau} \end{bmatrix}, \quad (3.32)$$

where \mathbf{J} is the Jacobian matrix which is expressed as,

$$[\mathbf{J}] = \begin{bmatrix} \sum_{i=1}^8 \left(\frac{\partial N_i}{\partial \xi} x_i \right) & \sum_{i=1}^8 \left(\frac{\partial N_i}{\partial \eta} x_i \right) & \sum_{i=1}^8 \left(\frac{\partial N_i}{\partial \tau} x_i \right) \\ \sum_{i=1}^8 \left(\frac{\partial N_i}{\partial \xi} y_i \right) & \sum_{i=1}^8 \left(\frac{\partial N_i}{\partial \eta} y_i \right) & \sum_{i=1}^8 \left(\frac{\partial N_i}{\partial \tau} y_i \right) \\ \sum_{i=1}^8 \left(\frac{\partial N_i}{\partial \xi} z_i \right) & \sum_{i=1}^8 \left(\frac{\partial N_i}{\partial \eta} z_i \right) & \sum_{i=1}^8 \left(\frac{\partial N_i}{\partial \tau} z_i \right) \end{bmatrix}, \quad (3.33)$$

where x_i , y_i and z_i refers to the coordinate positions of the node considered. The derivatives of shape

functions with respect to global coordinates is determined using Equation (3.32) and then assembled in Equation (3.31) to get the \mathbf{B} matrix.

For a geometrically linear analysis, the element stiffness matrix is defined as,

$$\mathbf{K}_e = \int_V \mathbf{B}^T \mathbf{D} \mathbf{B} dV, \quad (3.34)$$

$$dV = dx \cdot dy \cdot dz = \det(\mathbf{J}) d\xi \cdot d\eta \cdot d\tau,$$

where \mathbf{D} is the constitutive matrix that depends on the material parameters and the integration is performed over the reference (local) element. Gaussian quadrature is commonly used to perform numerical integration. The Gaussian quadrature is defined as,

$$\int_{-1}^1 \int_{-1}^1 \int_{-1}^1 f(\xi, \eta, \tau) d\xi d\eta d\tau = \sum_{i=1}^n f(\xi_i, \eta_i, \tau_i) w_i, \quad (3.35)$$

where n is the number of integration points chosen and w_i is the corresponding weight. n and w_i are fixed constants based on the type of Gauss quadrature used. The integration points and weights used are explained in Section 3.6.2.

3.4.2 FE Model - Neutral Angle Simulations

Using the node numbering of the element as presented in Figure (3.5), a hollow cylinder is generated using hexahedron elements as shown in Figure (3.6). The base mesh used in the simulations consists of 37525 nodes and 29704 elements.

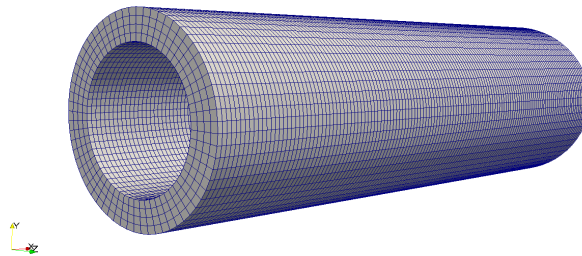


Figure 3.6: Volume model of a rubber hose.

To model the helical reinforcements within the volume model, the mesh is transformed such that the nodes are positioned in a helical manner. To perform this transformation, the mesh is rescaled such that the

total length is equal to the pitch length of the helix and each node is rotationally transformed about the axis of the hose depending on the position of the node along the same axis. In this case, each node is transformed about the x axis using the transformation,

$$R_x(\alpha) = \begin{bmatrix} 1 & 0 & 0 \\ 0 & \cos \alpha & -\sin \alpha \\ 0 & \sin \alpha & \cos \alpha \end{bmatrix}, \quad \alpha = \frac{x}{P} \cdot 2\pi, \quad (3.36)$$

where x is the length along the hose at which the node is present and 2π radians denoting the angle of one complete revolution of a helix. The resulting mesh of the hose is shown in Figure (3.7).

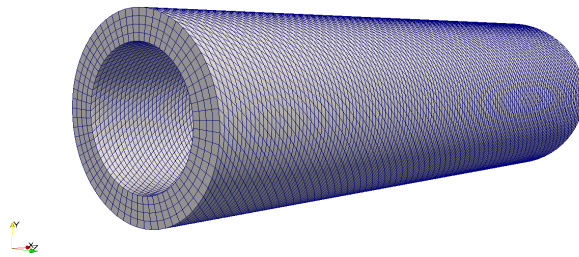


Figure 3.7: Helical volume model of a rubber hose.

Further, it is possible in LaStFEM to implement different elastic properties for each element in a model. Thus, one row or multiple row of elements can be picked from the default mesh which would denote a helical row after the transformation as illustrated in Figures (3.8) and (3.9) in which two rows of elements (highlighted in green) are used to represent a helical reinforcement. Properties of steel are given as input for these elements. The model could be considered as an extreme case of the smeared approach where the whole element is considered as a reinforcement.

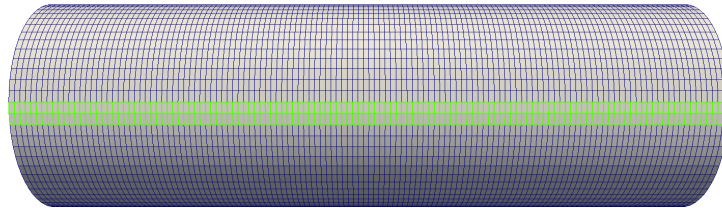


Figure 3.8: Row of elements in the default mesh.

Pressure is prescribed on the inner surface. To account for the effect of closed ends, the end force as given

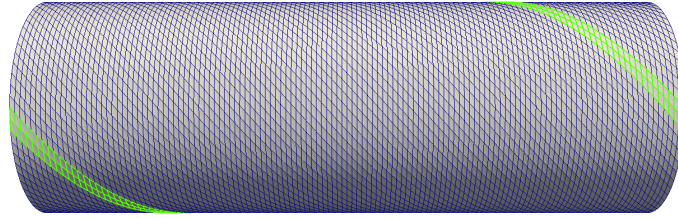


Figure 3.9: Row of elements after transformation.

in Equation (3.2), is divided by the total number of nodes at the end surface and prescribed in the axial direction for each of those nodes. Similar boundary conditions are implemented as used for the beam model of the reinforcement. The left end is fully constrained whereas the right end is free to move in axial direction alone. Also, steel properties are implemented for all the elements on the surfaces of both the ends to simulate the effect of stiff end caps.

Several alternatives for the representation of the reinforcements are implemented. The number of rows denoting a reinforcement is varied or all the elements through the thickness are picked to denote a reinforcement. For each case, the effect of neutral angle is studied by varying the helix angle and determining change in length.

3.5 Coupled Model

There have been many approaches to model reinforcements as discussed in Chapter 2. To model the localized interactions of the reinforcements, it would be better to model the reinforcements separately with their own degrees of freedom and introduce constraints on the model such that the volume model of the rubber and the truss model of the reinforcement are coupled. A simple way to couple a 3D model with a 1D model is to introduce a spring constraint on the nodal displacements or positions of the corresponding nodes. Consider a volume element with a reinforcement node inside it as shown in Figure (3.10).

The displacement of the truss node is denoted as \mathbf{u}_T and the interpolated displacement of the volume element is denoted as \mathbf{u}_V . The constraint condition is such that the displacement of the truss node is equal to the interpolated displacement. A spring force will act on these nodes if these displacements are different,

$$\begin{aligned} \mathbf{f}_T &= -\kappa(\mathbf{u}_T - \mathbf{u}_V), \\ \mathbf{f}_V &= \kappa(\mathbf{u}_T - \mathbf{u}_V), \end{aligned} \tag{3.37}$$

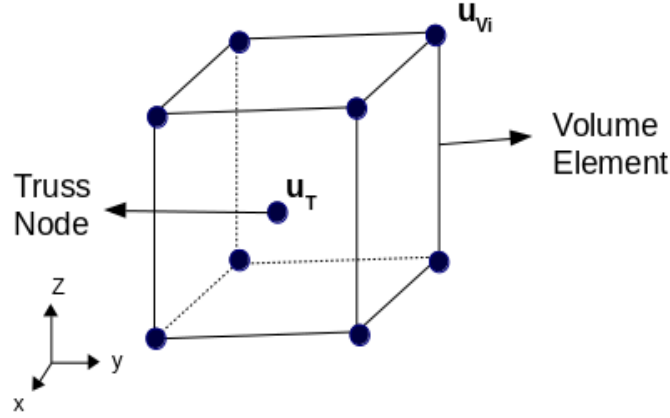


Figure 3.10: Schematic of a reinforcement node within a volume element.



Figure 3.11: Imaginary spring connecting the truss node and the volume node.

where κ is the spring constant. The value of κ should be chosen sufficiently high for the coupling to work effectively. The displacement of the volume element can be interpolated from the nodes as,

$$\mathbf{u}_V = \sum_{i=1}^8 N_i \mathbf{u}_{V_i}. \quad (3.38)$$

Similarly, the forces on the truss and volume nodes for the imaginary spring element (see Figure 3.11) is given by,

$$\begin{aligned} \mathbf{f}_T &= -\kappa(\mathbf{u}_T - N_i \mathbf{u}_{V_i}), \\ \mathbf{f}_{V_j} &= N_j \kappa(\mathbf{u}_T - N_i \mathbf{u}_{V_i}) \quad , i, j = 1, \dots, 8. \end{aligned} \quad (3.39)$$

To find the contribution of the coupling to the stiffness matrix, the forces \mathbf{f}_T and \mathbf{f}_V have to be differentiated with respect to the displacements \mathbf{u}_T and \mathbf{u}_V resulting in,

$$\begin{aligned} \delta f_{TT} &= -\kappa \cdot I \delta \mathbf{u}_T, \\ \delta f_{TV} &= \kappa N_i \delta \mathbf{u}_V, \\ \delta f_{VT} &= \kappa N_j \delta \mathbf{u}_T, \\ \delta f_{VV} &= -\kappa N_i N_j \delta \mathbf{u}_V. \end{aligned} \quad (3.40)$$

Thus, the local stiffness matrix for the truss and volume nodes due to the spring constraint will be,

$$\mathbf{K} = \begin{bmatrix} -\kappa I & \kappa N_i \\ \kappa N_j & -\kappa N_i N_j \end{bmatrix}. \quad (3.41)$$

The force and stiffness contributions should be added for each truss node. LaStFEM has a functionality, if given a arbitrary point, it would return the element within which it is located, the nodes of the respective element and the local coordinates ξ, η, τ of the point. Thus, for each truss node, the element which contains the point and its nodes can be determined. An element routine is developed which would calculate the force and stiffness contributions for each truss node and the nodes of the volume element within which it is present. The values would be added to the corresponding nodal values.

Using the coupling between the volume model for rubber and the truss model for reinforcements, the neutral angle simulations are performed with the same loads and boundary conditions as mentioned in Section 3.4.2. The FE model in which reinforcements are implemented in two directions is presented in Figure (3.12). Equation (2.1) is used with positive and negative sign for y to define helices in both directions. Further, to get multiple helices, a rotational transformation is performed on all nodes as mentioned in Equation (3.36) with $\alpha = \frac{2\pi}{n}$ where n is the number of helices required.

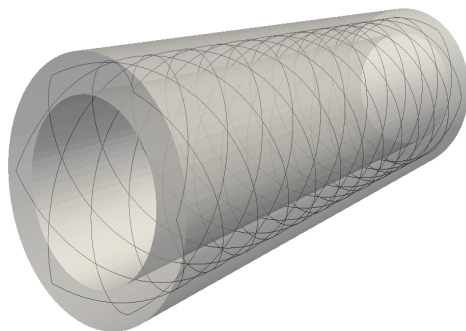


Figure 3.12: FE setup with truss model inside the volume model.

A mesh convergence study is also performed with four different meshes. The nodes and elements in each mesh is given in Table (3.1). Mesh 2 has been used in all other simulations.

3.6 Embedded Model

Consider helical reinforcements passing through the rubber hose (modeled in 3D). To implement the embedded model, the volume elements through which the reinforcements passes should be determined.

Table 3.1: Various meshes used with number of nodes and elements.

Mesh	Nodes	Elements
1	23600	18644
2	37525	29704
3	52535	44556
4	94446	83160

Further, the length of the reinforcement within each crossed element and the way in which the reinforcements are orientated should be given as input. This could be effectively implemented if the nodes of the reinforcement model are considered to be positioned at the intersections with the volume model. From the nodal positions, the length and the orientations could be obtained. Thus, a mesh intersection algorithm developed by Raul et al [34] is used to get the intersection points between the 3D model and helical curve.

3.6.1 Mesh Intersection Algorithm

The methods involves three key procedures:

- Inverse mapping to find local coordinates.
- Boundary functions to locate whether the point is inside or outside an element.
- Bisection method to locate intersections.

3.6.1.1 Inverse Mapping

Inverse mapping is the method used to compute the local coordinates ξ of a point with spatial coordinates \mathbf{x} . The method involves the use of the Newton-Raphson scheme since it provides quadratic convergence. For an isoparametric element, the spatial coordinates $\mathbf{x}(\xi)$ are determined by,

$$\mathbf{x}(\xi) = \sum_i N_i(\xi) \mathbf{x}_i, \quad (3.42)$$

where $N_i(\xi)$ are the interpolation functions of the particular element, i is the number of nodes and \mathbf{x}_i is the nodal coordinates of the element. To find the local coordinates of a spatial point \mathbf{x}_{in} , the procedure starts with a guess value of the local coordinates ξ_{trial} and finding the approximated value from Equation (3.42) using ξ_{trial} . The residual to find ξ is,

$$\mathbf{r}(\xi) = \mathbf{x}_{in} - \sum_i N_i(\xi) \mathbf{x}_i. \quad (3.43)$$

The Jacobian of the residual is defined as,

$$\mathbf{J}(\xi) = \frac{d\mathbf{r}}{d\xi} = - \sum_i \mathbf{x}_i \otimes \frac{dN_i(\xi)}{d\xi}. \quad (3.44)$$

If the residual is zero, then the local coordinate of the spatial point \mathbf{x}_{in} is found. Else, Newton iterations are performed to update the value of ξ . The updated ξ is found using,

$$\xi^{k+1} = \xi^k - \mathbf{J}^{-1} \mathbf{r}^k. \quad (3.45)$$

The iterations are repeated until the norm of the residual is less than a specified tolerance value.

3.6.1.2 Boundary Function

Boundary functions are used to find whether a point is located inside, outside or at the boundary of the element. The local coordinates ξ of a spatial point is used as an input to the boundary function. The boundary functions are devised in such a way that it returns a positive value if the point is located inside the element, a negative value if it is located outside the element and zero if it is located at the boundary of the element. The boundary function for a quadrilateral element can be visualized as shown in Figure (3.13). The boundary functions for quadrilateral and hexahedral elements are given as,

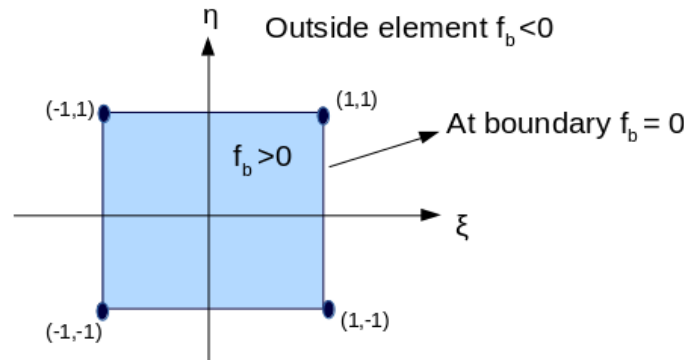


Figure 3.13: Boundary Function for a Quadratic element.

$$\begin{aligned} f_b^{quad} &= \min(1 - |\xi|, 1 - |\eta|), \\ f_b^{hex} &= \min(1 - |\xi|, 1 - |\eta|, 1 - |\tau|). \end{aligned} \quad (3.46)$$

3.6.1.3 Bisection Method

The 1D model that is embedded within the volume element should be defined by parametric equations, (in this case Equation (2.1)). The points of these equations are the required inputs for this method to find the intersections. The procedure will be explained with the help of a 2D example as shown in Figure (3.14). A line passes through a 2D mesh with a parameter s . For a value of $s \in [0,1]$, the corresponding

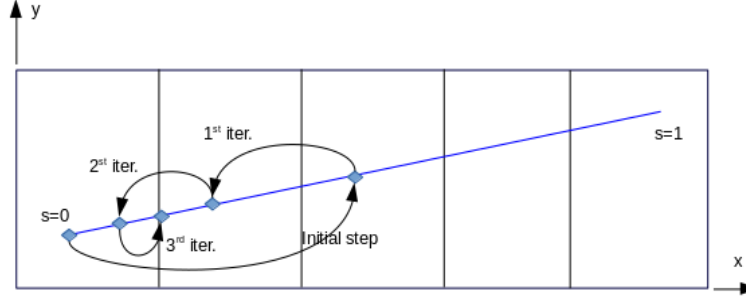


Figure 3.14: Intersection determination using Bisection method.

spatial coordinates can be found using the parametric equations. Using LaStFEM's functionality, the element that contains the first point s_0 of a curve or a line is determined.

To check if a spatial point with local coordinates ξ^e is within a particular element e , then it should satisfy the relation,

$$f_b(\xi^e) \geq \varepsilon_c \quad (3.47)$$

where f^b is the boundary function and ε_c is a tolerance which ensures that the point that is lying on the boundary is considered as located inside the element e .

After the first crossed element e_0 is found, the procedure continues to find the first intersection point s_1 that is located at the boundary of e_0 . The first trial point would be located at the midpoint of the curve or line. Several trial points, s_{tr} , will be tested along the curve. The first intersection point would be the one with $f^b(\xi(s_{tr})) = 0$, thus $s_1 = s_{tr}$. As per the bisection method, the number of iterations required to find the intersection point is given by,

$$n_{iter} = \text{trunc} \left[\log_2 \left(\frac{\Delta s}{\varepsilon_b} \right) \right] + 1, \quad (3.48)$$

where ε_b is a tolerance that represents a ratio of the curve length and the first trial point being $s_{tr} = s_0 + \Delta s$. Trunc refers to considering only the integer value of the expression given within the brackets. In each successive iterations, the step size will be reduced by half ($\Delta s \rightarrow \Delta s/2$). Further if the trial point is located within the element, the trial point would be moved forward in the next iteration ($s_{tr} \rightarrow s_{tr} + \Delta s$) and if the point is located outside the element, the trail point would be moved backward ($s_{tr} \rightarrow s_{tr} - \Delta s$).

Once the first intersection point s_1 is determined, the next crossed element e_1 should be found. A small increment ϵ is added to the parametric coordinate and the element that contains this point is found using LaStFEM. The value of ϵ should be chosen with care so that none of the elements are ignored in the jump due to the ϵ . Now, the initial step would be half of the remaining curve length. The procedure is repeated until all the points are determined. When all intersection points are found, the curve end would be reached.

In the case of a helix passing through the rubber hose model, from the parametric equation of a helix

(Equation (2.1)), $t \in [0, n_r \cdot 2\pi]$ radians can be used a suitable parameter, where n_r is the number of revolutions in the helix.

The method has been summarized below,

Algorithm 1 Mesh Intersection algorithm

- 1: Get the parametric coordinate of the first point.
 - 2: Through inverse mapping, determine the local coordinates of the first point.
 - 3: Using LaStFEM, find the element containing the first point.
 - 4: Implement bisection method using boundary function in a iterative process to find the intersection point.
The number of iterations required is calculated using Equation (3.48).
 - 5: Find the next crossed element using the tolerances.
 - 6: Repeat the procedure till the last point of the curve.
-

3.6.2 Stiffness contribution of Reinforcement

As mentioned in Section 2.3.3, the stiffness contribution of the reinforcement would be added to the element stiffness matrix of the rubber model. The element stiffness matrix is modified as,

$$\mathbf{K}_e = \mathbf{K}_{m,e} + \sum_{i=1}^{N_r} \mathbf{K}_{r,i,e}, \quad (3.49)$$

where $\mathbf{K}_{m,e}$ denotes the stiffness contribution of rubber hose and described in Equation (3.34). For a linear analysis, the element stiffness matrix of reinforcement is given as,

$$\mathbf{K}_{r,i,e} = A_i \int_{S_i} \mathbf{B}^T \mathbf{C}_i^T \mathbf{D}_i \mathbf{C}_i \mathbf{B} ds, \quad (3.50)$$

where A_i represents the cross sectional area of the reinforcement, S_i represents the length of the reinforcement within the element, \mathbf{B} is the strain displacement matrix as defined in Equation (3.31) and \mathbf{C}_i is the matrix that links the strains of the reinforcements with that of the matrix material, given as,

$$\mathbf{C} = \begin{bmatrix} l^2 & m^2 & n^2 & lm & mn & ln \\ 0 & 0 & 0 & 0 & 0 & 0 \\ 0 & 0 & 0 & 0 & 0 & 0 \\ 0 & 0 & 0 & 0 & 0 & 0 \\ 0 & 0 & 0 & 0 & 0 & 0 \\ 0 & 0 & 0 & 0 & 0 & 0 \end{bmatrix}, \quad (3.51)$$

where l, m, n are the direction cosines in x, y, z directions. If (x_1, y_1, z_1) and (x_2, y_2, z_2) represent the initial and the end points of the reinforcement within an element, then a vector joining these two vectors can be expressed as,

$$\begin{aligned} \mathbf{v} &= v_x \mathbf{e}_x + v_y \mathbf{e}_y + v_z \mathbf{e}_z, \\ v_x &= x_2 - x_1, v_y = y_2 - y_1, v_z = z_2 - z_1. \end{aligned} \quad (3.52)$$

The direction cosines is defined by,

$$\begin{aligned} l &= \frac{v_x}{\sqrt{v_x^2 + v_y^2 + v_z^2}}, \\ m &= \frac{v_y}{\sqrt{v_x^2 + v_y^2 + v_z^2}}, \\ n &= \frac{v_z}{\sqrt{v_x^2 + v_y^2 + v_z^2}}. \end{aligned} \quad (3.53)$$

The reinforcement is considered to contribute to the stiffness matrix only in the longitudinal direction. Thus, the \mathbf{D} matrix is given by,

$$\mathbf{D} = \begin{bmatrix} E_r & 0 & 0 & 0 & 0 & 0 \\ 0 & 0 & 0 & 0 & 0 & 0 \\ 0 & 0 & 0 & 0 & 0 & 0 \\ 0 & 0 & 0 & 0 & 0 & 0 \\ 0 & 0 & 0 & 0 & 0 & 0 \\ 0 & 0 & 0 & 0 & 0 & 0 \end{bmatrix}, \quad (3.54)$$

where E_r is the Young's modulus of the reinforcement. The integration in Equation (3.50) should be performed at quadrature points along the reinforcement and not on the quadrature points of the solid element. A three point quadrature is used to perform the integration. The points and weights are given in Table (3.2).

Table 3.2: The points and weights in three point quadrature.

n	Point	Weight
1	0	$\frac{8}{9}$
2	$+\sqrt{\frac{3}{5}}$	$\frac{5}{9}$
3	$-\sqrt{\frac{3}{5}}$	$\frac{5}{9}$

The reinforcement is considered in 1D and vary from -1 to 1 in its local coordinates. The length of the reinforcement in global coordinates is mapped to the local coordinate values and these three integration points are determined.

To implement the embedded model, user defined elements are created with the same nodes as the solid elements through which the reinforcements passes. For each of these elements, the stiffness contribution of the reinforcements are determined using the procedure above. Further, the internal force contributions are determined using,

$$\mathbf{F} = \mathbf{K}\mathbf{a}, \quad (3.55)$$

where \mathbf{a} is the nodal displacements of the element.

The neutral angle simulations are performed with a setup as shown in Figure (3.6). The boundary conditions and the loads are the same as mentioned in Section 3.4.2.

3.7 Abaqus Model

As an example of modeling reinforcements with a commercial solver, the reinforced hose is modeled in Abaqus. There is an embedded constraint in Abaqus [32], which models reinforcements by eliminating the degrees of freedom for the reinforcements. The host model is the model within which the reinforcements are embedded. If a node of an embedded element lies within a host element, the translational degrees of freedom of the node are eliminated and the node becomes an “embedded node.” Embedded elements are allowed to have rotational degrees of freedom, but these rotations are not constrained by the embedding. This is similar to the models that have been implemented in this work but the exact solving procedure in Abaqus is unknown.

3.7.1 FE Model - Neutral Angle Simulations

A three-dimensional model has been created for rubber by drawing a circle and extruding it. Hexahedron elements are used to mesh the model as shown in Figure (3.15).

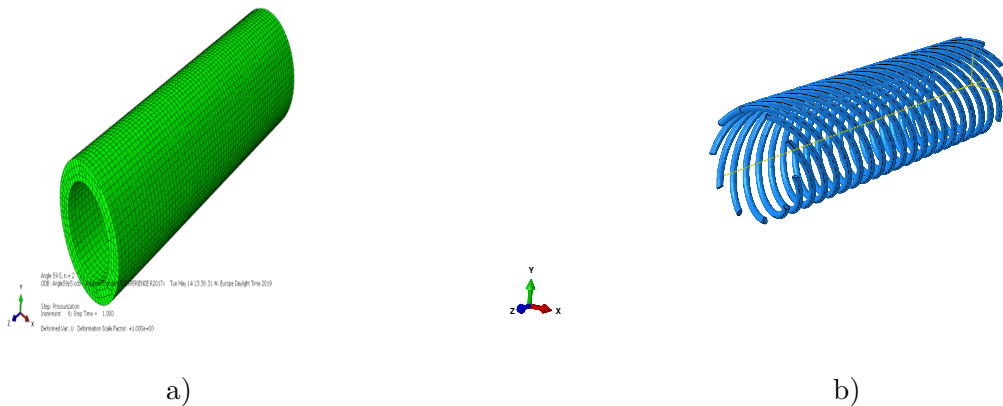


Figure 3.15: Abaqus model of a) Rubber Hose b) Reinforcement.

Further, using revolution a three-dimensional helical structure is obtained. A three-dimensional reinforcement is embedded within a three-dimensional rubber hose model. Circular pattern is used to create multiple helices. An assembly with both the models has been created as shown in Figure (3.16) along with embedded constraints which defines the hose model as the host element and the reinforcement as embedded element. To study the effect of the neutral angle, similar boundary conditions are implemented as performed for simulations before as mentioned in Section 3.4.2. Pressure is prescribed on the inner surface and end forces are applied as surface traction at the end surface.

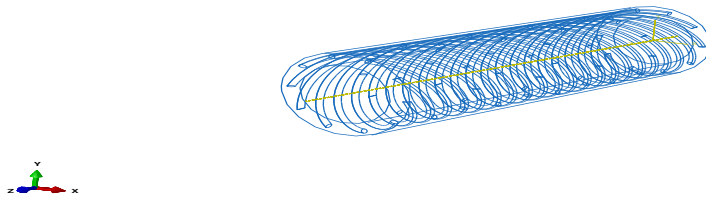


Figure 3.16: Assembly of Rubber Hose and Reinforcement.

3.8 Bending Simulation

Two different methods are considered to study the bending stiffness behaviour of a pure rubber hose model and a reinforced hose model.

3.8.1 Three Point Bending Setup

A setup as described in Figure 1.2 is used in this case. The force required to displace the hose is measured. From these values, it is possible to derive the bending stiffness value (EI) by considering Euler-Bernoulli beam theory for a simply supported beam with central load as,

$$\frac{dF}{dw} = \frac{48EI}{L_s^3}, \quad (3.56)$$

where dF is the force required to displace the hose by dw , I is the second moment of inertia of the hose and L_s is the distance between the supports. The moment of inertia for a hollow circular cross section with an outer radius R_o and inner radius R_i is given by,

$$I = \frac{\pi}{4}(R_o^4 - R_i^4). \quad (3.57)$$



Figure 3.17: Three point bending FE model.

The FE model used for a three point bending setup is shown in Figure (3.17). A rubber hose with a length of 0.343 m is considered with the supports separated by a distance of 0.15 m. Rigid objects are placed at the ends of the hose. These objects would be in contact with the nodes at the end surfaces of the hose. Rigid objects have one node each with three translational degrees of freedom and three rotational degrees of freedom which would enable the model to rotate about the z-axis. Contacts are defined similarly with the supports also. Pressure is prescribed in the inner surface and end forces are prescribed on the rigid objects such that they will always act in a direction normal to the hose end.

In the experimental setup, there is a clamp present at the centre of the hose onto which the force is prescribed. The region of the hose under the clamp does not expand during pressurization. Thus, to have a similar setup, nodes in the outer surface at the centre of the rubber model are fully constrained. Displacements will be prescribed on these nodes and reaction forces are extracted for each displacement step. Mesh 2 has been refined length wise to have better resolution for the region near the supports for this case resulting in 75050 nodes and 59724 elements.

3.8.2 MeSOMICS Setup

Fraunhofer ITWM has developed an experimental setup called MeSOMICS [35]. MeSOMICS stands for Measurement System for the Optically Monitored Identification of Cable Stiffnesses. It is proven to be a robust method to determine the stiffness of a hose when compared to the standard three point bending test. Moreover, the test allows the hose to have a relevant radii of curvature. Using the curved hose, displacements are prescribed at one end to bend it and forces are measured. The experimental setup is shown in Figure (3.18). To setup a FE model to mimic the MeSOMICS experiment, a curved model of a

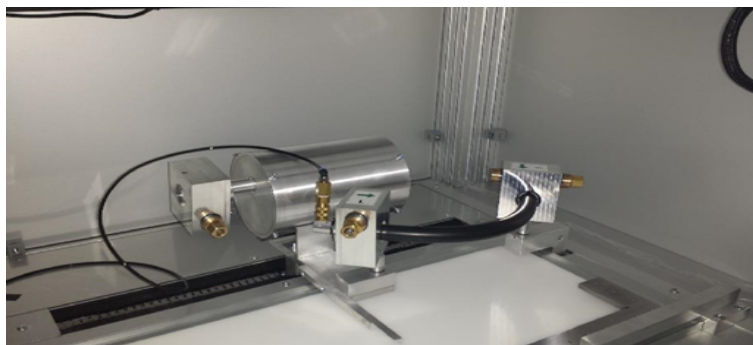


Figure 3.18: Experimental Setup.

rubber hose model is required. Thus, the following transformation is implemented on a straight rubber hose model.

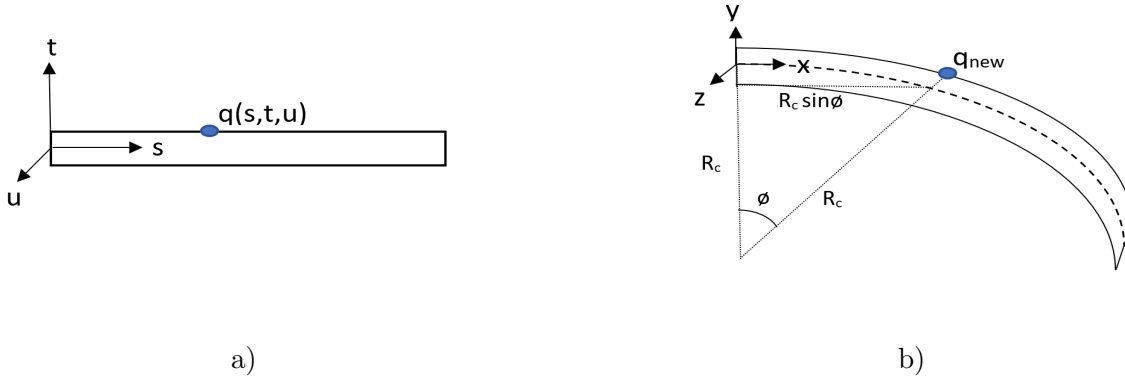


Figure 3.19: Transformation to form a curved model. a) A point on the straight model. b) The same point on the curved model.

Consider a point $q(s, t, u)$ in the default configuration of the hose. The hose is transformed to a curved one with a radius R_c , as presented in Figure (3.19). Using trigonometry, the new coordinates of the point q is found to be $[(R_c + t)\sin \phi, -R_c(1 - \cos \phi) + t \cos \phi, u]$. A constraint $s = \phi R_c$ is employed to enforce compatibility resulting in,

$$q_{new} = [(R_c + t)\sin \phi, -R_c(1 - \cos \phi) + t \cos \phi, u] = \left[(R_c + t)\sin \left(\frac{s}{R_c} \right), -R_c \left(1 - \cos \left(\frac{s}{R_c} \right) \right) + t \cos \left(\frac{s}{R_c} \right), u \right]. \quad (3.58)$$

Thus, for each node in the default configuration, the transformation is employed to get the new curved model required for the setup. The FE model is presented in Figure (3.20).

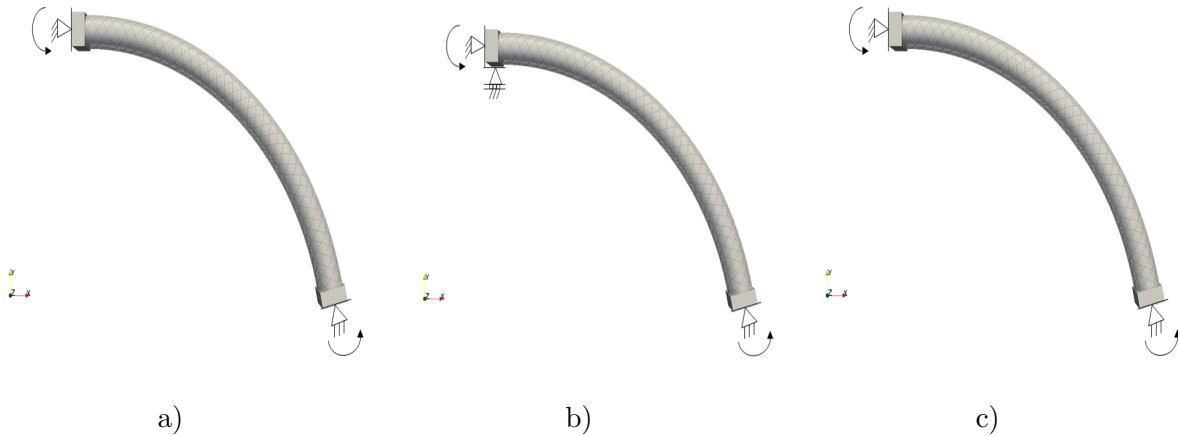


Figure 3.20: MeSomics FE Model. a) Setup 1: Constrained pressurization. b) Setup 2: Unconstrained pressurization during pressurization step. c) Setup 2: Unconstrained pressurization during displacement steps.

A straight hose with a length of 0.267 m, approximately equal to the length used in experiments is bent with a radius of 0.2 m. Rigid objects are used in the setup similar to three point bending setup. The boundary conditions and forces will be prescribed on these nodes. MeSOMICS simulations consists of a pressurization step and a displacement step. Two different setups are used, namely constrained pressurization and unconstrained pressurization. In constrained pressurization (Figure 3.20 a), all degrees of freedom are constrained except for a rotational degree of freedom about the z-axis throughout the simulation. The hose is not allowed to expand or deform during pressurization. In unconstrained pressurization, during pressurization (Figure 3.20 b), apart from free rotation about z-axis, the model is free to translate along the hose axis. The hose is locked at its new position for the displacement steps (Figure 3.20 c) with free rotation about z-axis. The boundary conditions are illustrated in the figures to differentiate between the two setups. Pressure is prescribed in the inner surface and end forces are prescribed on the rigid objects. Displacements are prescribed at one node in a direction of a line joining these two nodes. Reaction forces are extracted for each displacement step from the node in which displacements are prescribed.

3.9 Torsion Simulation

To determine the torsional stiffness of the hose, a standard torsion setup is used in the FE model as presented in Figure (3.21).



Figure 3.21: Torsion FE Model.

A length of 0.07 m is used. As in bending, rigid objects are placed at the ends. Pressure and end forces are prescribed as performed in the bending simulation. The node of one of the rigid objects is fully constrained. The other rigid object's node would have all its degrees of freedom constrained except of translation in the hose axis. This boundary condition enables the hose to extend or contract during pressurization. After pressurization, the angle of twist is prescribed at the end which is free to move. For each angle, the reaction moment is extracted.

4

Results & Discussions

The results obtained from the models that have been implemented are presented in this chapter. Further, the results are analyzed and the capabilities of the models are discussed.

4.1 Beam Model - Neutral Angle Simulations

Initially, the beam model is studied for two different helix angles 50° and 60° . The initial setup and the deformed model are presented in Figure (4.1). The model is generated by using Equation (2.1) in which nodes are placed at each degree between 0° and 360° (which will be converted in terms of radians).

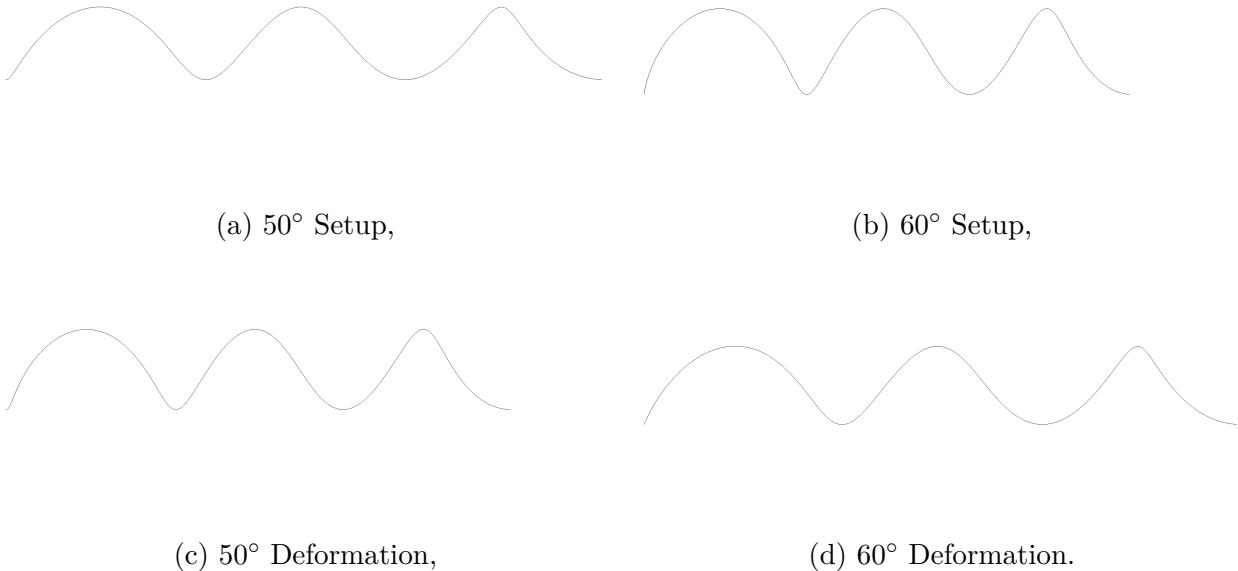


Figure 4.1: Beam model setup and deformation.

It is observed that, for a helix angle of 50° , the model is contracting and for a helix angle of 60° , the model

is expanding. There exists a neutral angle between these values at which there would be no deformation. To find the value of the neutral angle, a parametric study is performed by varying the angle in each simulation and extracting the change in length for each angle. A refined mesh with twice the resolution is also considered. Models with different helix radius are also studied to see if the neutral angle depends on the helix radius. The results obtained for a pressure of 1 bar are shown in Figure (4.2).

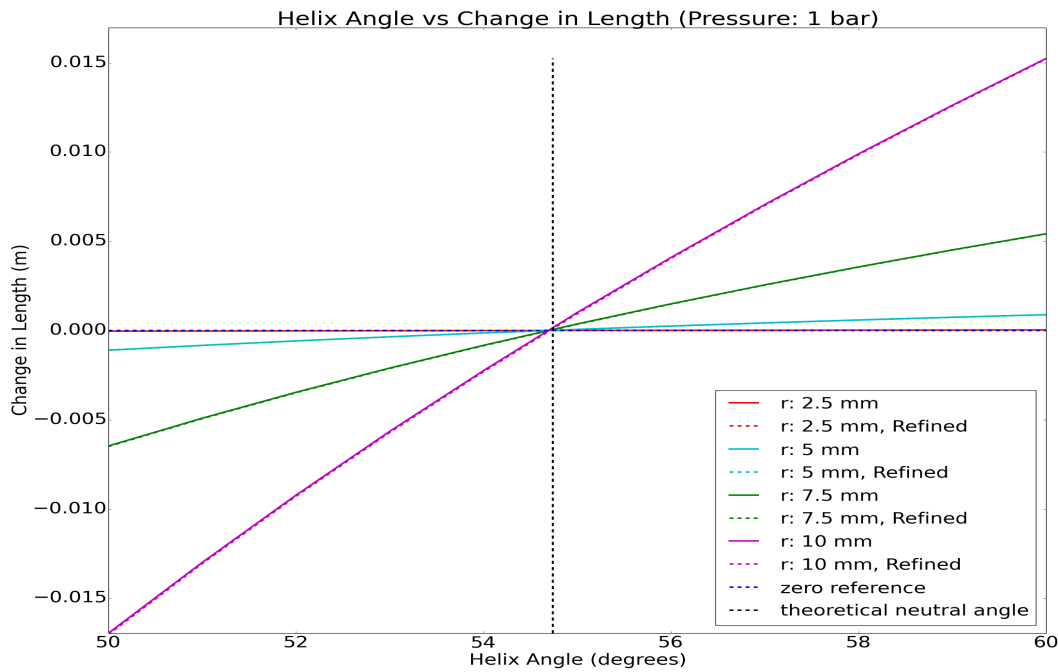


Figure 4.2: Results of beam model for 1 bar pressure.

For all the cases, it has been observed that the neutral angle remains constant and has a value which is very close to the theoretical value denoted by the dotted black line. It is also evident that the neutral angle does not depend on the helix radius and the solutions does not change with a refined mesh. Further, two models, with a helix radii of 5 mm and 7.5 mm are chosen to be studied for higher pressures of 3 bar, 5 bar and 10 bar. The results are presented in Figure (4.3).

The results show that the neutral angle does not vary if pressure is increased as expected since the derivation of the neutral angle does not depend on pressure level. The main idea behind the model is to investigate whether beam models could be used to model reinforcements and the results show that the beam model accurately captures the effect of the neutral angle.

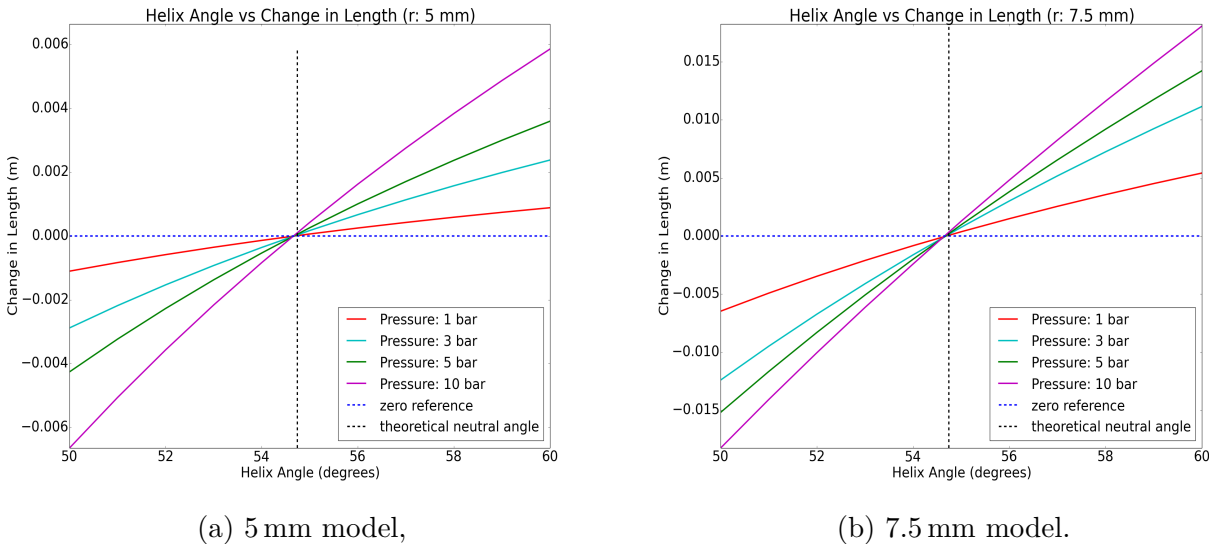


Figure 4.3: Results of beam model for varying pressures.

4.2 Truss Model - Neutral Angle Simulations

The parametric study as explained in the previous section is repeated for the truss model. The results are compared with a beam model with a helix radius of 10 mm and 20 mm to check the difference between these models. In each case, the number of revolutions are modified which is denoted N in Figure (4.4).

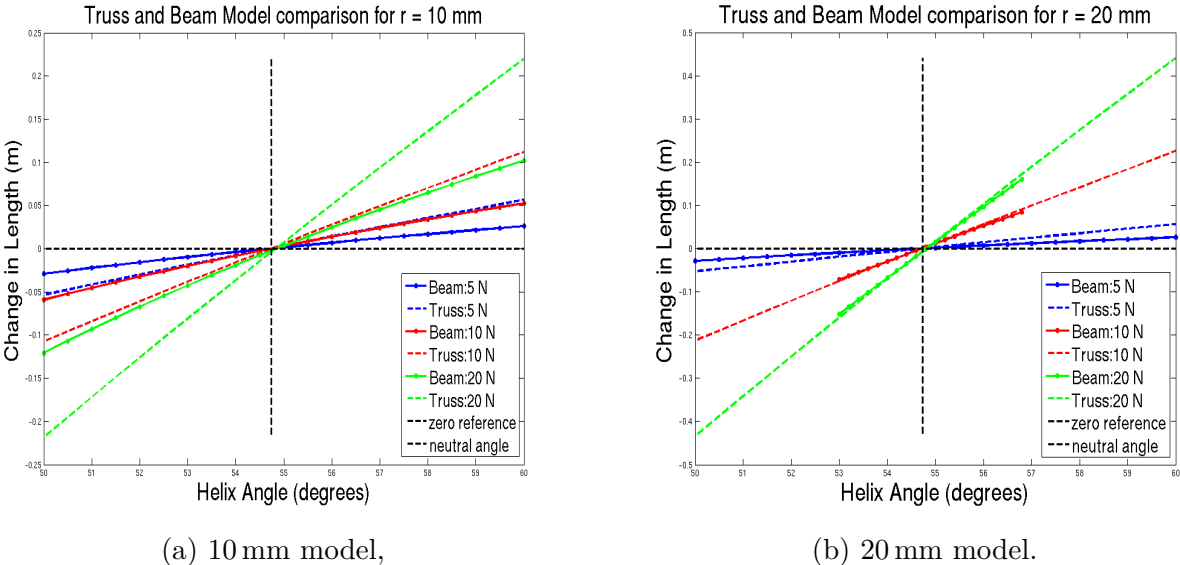


Figure 4.4: Comparison between truss and beam model.

For helix radius 10 mm, it is seen that there are some differences between the results of the two models whereas for helix radius 20 mm and with more number of revolutions, the results of the truss model and the beam model agree with each other. The reason behind is that, under these conditions, the effect of bending would be minimal or negligible, which makes the results similar. For lower helix radius and lower length (less number of revolutions), due to the boundary condition (one end is completely fixed, while the other is free to translate), there might be local bending associated with the beam model that causes the deviation. From these results, it can be inferred that truss model is also suitable to model isolated reinforcements.

4.3 Volume Model - Neutral Angle Simulations

In the volume model, several variants for reinforcements have been implemented and the results are shown in Figure (4.5). Two helices with four rows (2h4r), four helices with four rows (4h4r) and eight helices with two rows (8h2r) for pressure levels of 1 bar and 10 bar have been plotted. The models can be considered as having reinforcements with different cross sections or as several reinforcements put together to form one helix.

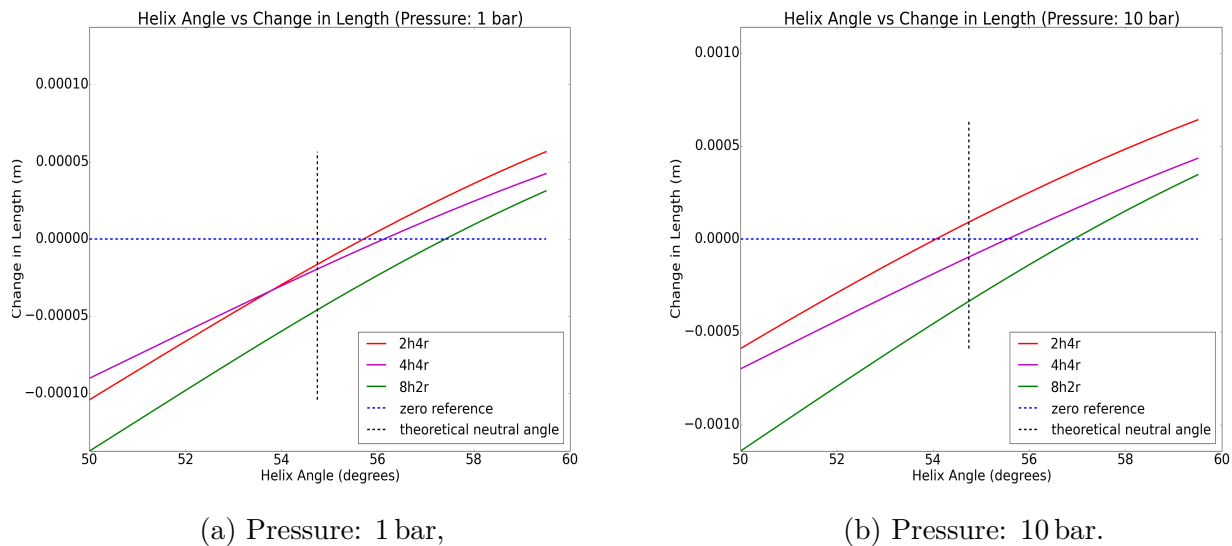


Figure 4.5: Results of beam model for varying pressures.

It could be seen that the model is able to capture the effect of a neutral angle, but the neutral angle is varying for each model. Moreover, with increase in pressure, deviations in the neutral angle has been observed. The strain contours for 10 bar case is presented in Figure (4.6). The strain contours shows that there is a considerable amount of bulging that occurs in the elements which corresponds to the rubber material. But, the elements with steel has very little strain (indicated in dark blue). This leads to a non-uniform deformation that depends on the number of steel elements in the model. This causes the deviation in the neutral angle for higher pressures.

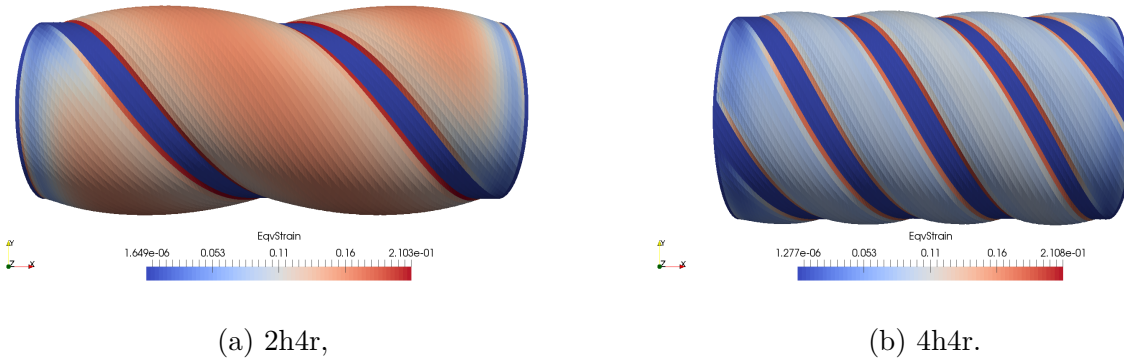
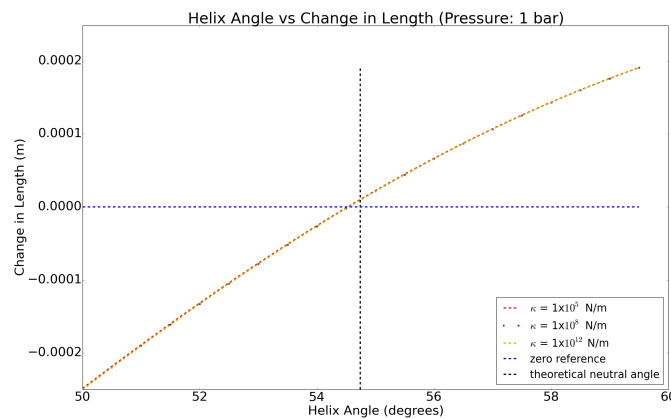


Figure 4.6: Strain contours of volume model.

The model can be twisted such that it is possible to model only one revolution and a very fine mesh would be needed to model more revolutions. The model has several limitations, but the neutral angle effect can be observed.

4.4 Coupled Model - Neutral Angle Simulations

At first, coupled model with 4 helices is considered with different values of spring constant to check whether the solution depends on it. As shown in Figure (4.7), there is a slight deviation in the results for values between 10^5 N/m and 10^8 N/m whereas the results are found to be exactly same for values 10^8 N/m and 10^{12} N/m. Thus, $\kappa = 10^8$ N/m is found to be suitable and has been used for rest of the simulations.

Figure 4.7: Results of coupled model for different κ values.

The setup and deformation of the reinforcements and the rubber model is shown in Figure (4.8).

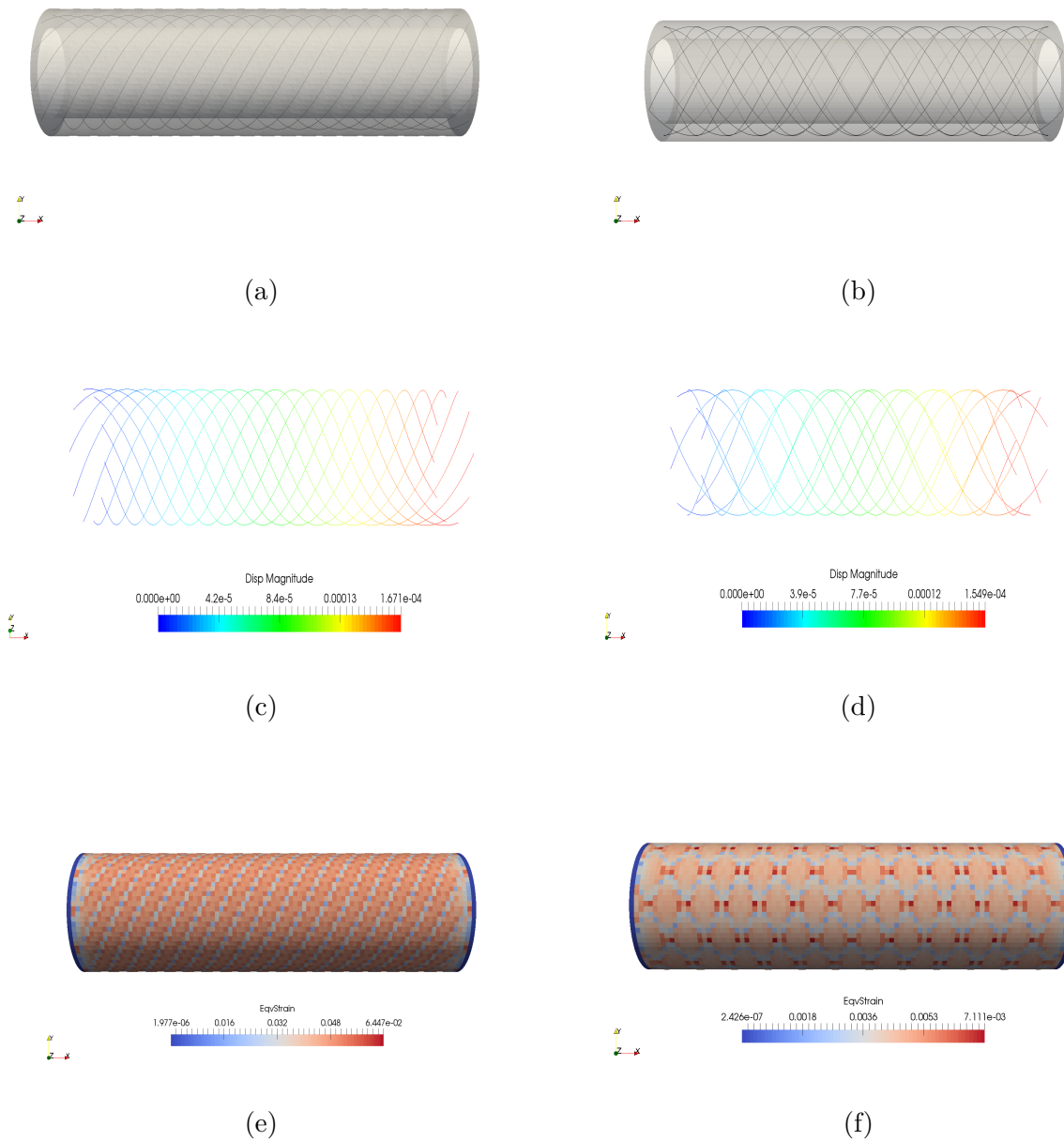


Figure 4.8: Coupled model deformation in neutral angle simulations. a) Model setup with reinforcements in one direction, b) Model setup with reinforcements in two directions, c) Displacement for reinforcements in one direction, d) Displacement for reinforcements in two directions, e) Strain in the rubber model with reinforcements in one direction, f) Strain in the rubber model with reinforcements in two directions.

The helical patterns are visible in the displacement contours of the rubber model. The results from neutral angle simulations for 1 bar pressure level with reinforcements in one direction are presented in Figure (4.9).

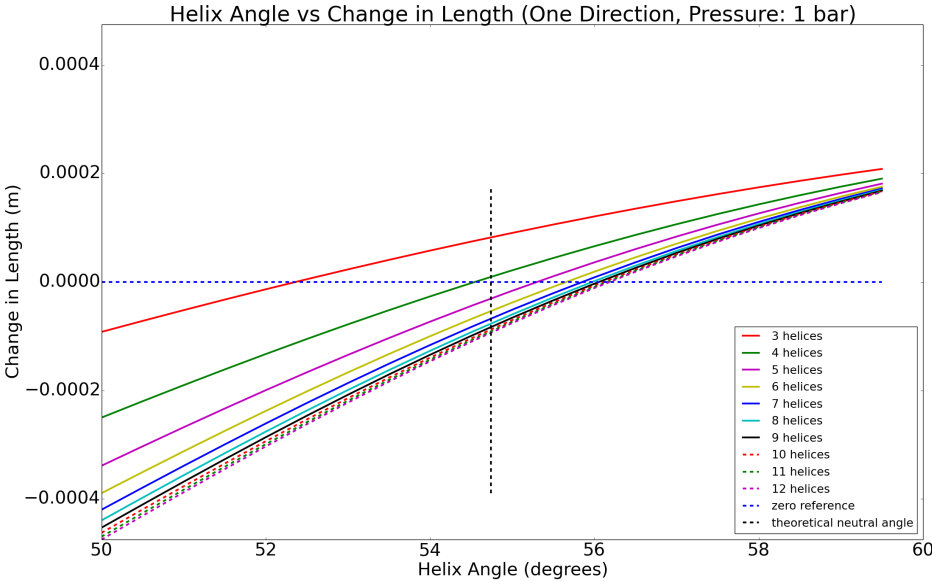


Figure 4.9: Results of coupled model for 1 bar pressure with reinforcement in one direction.

In each model, the number of reinforcements is increased. It can be seen that with an increase in the number of reinforcements in the model, the neutral angle is converging towards 56° that is closer to the theoretical value of 54.74° . A similar behaviour is seen for reinforcements in two directions as well as shown in Figure (4.10), with the neutral angle converging towards 56° .

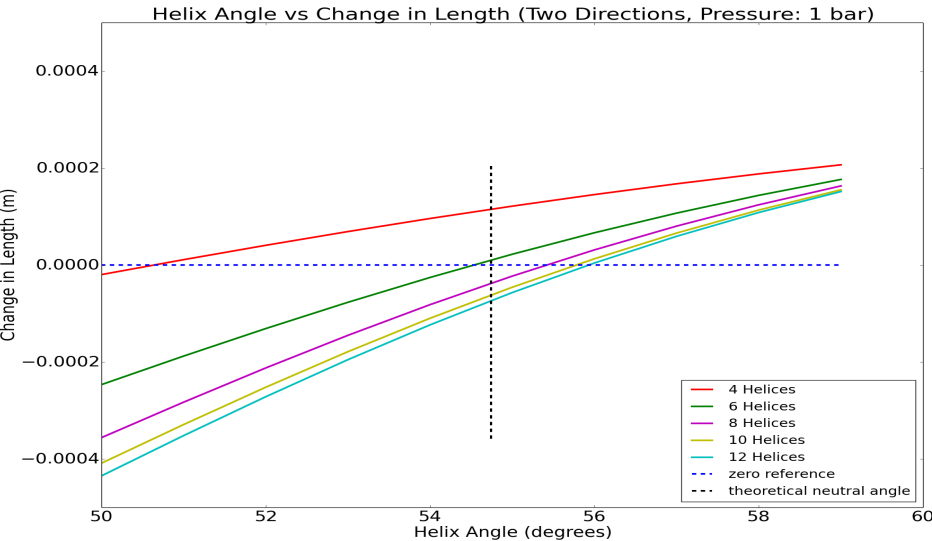


Figure 4.10: Results of coupled model for 1 bar pressure with reinforcement in two directions.

4. Results & Discussions

A mesh convergence study has been performed for two models with 4 and 10 helices for 1 bar pressure level with reinforcement in one direction. The results are shown in Figure (4.11). The results are found to be varying for the model with 4 helices whereas the deviations are minimal for the model with 10 helices.

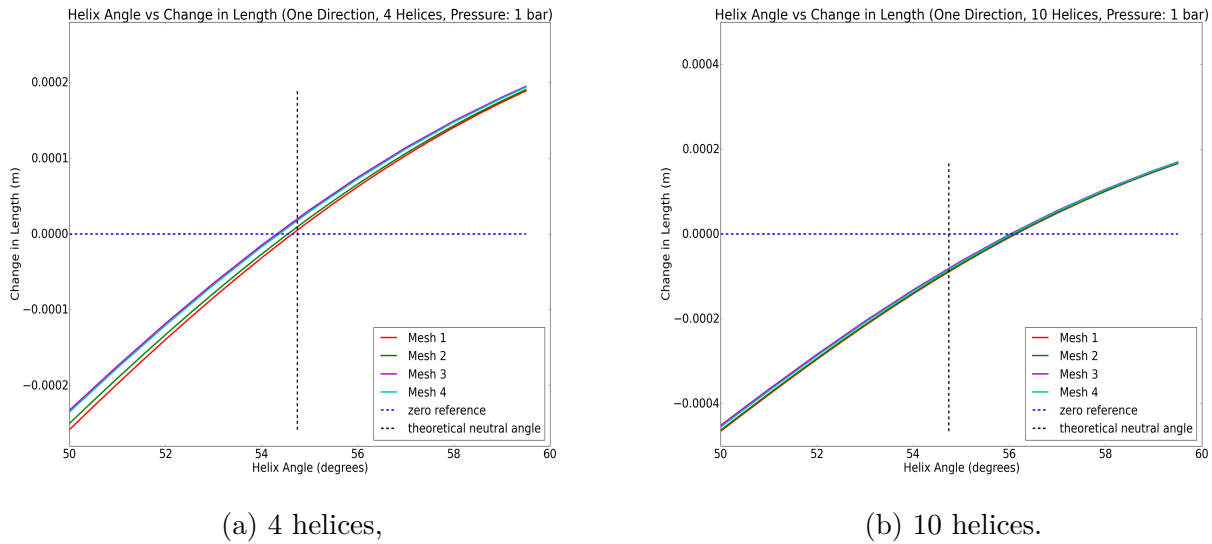


Figure 4.11: Mesh convergence study of the coupled model for 1 bar pressure.

For higher pressures, results are presented in Figure (4.12) for two models with 4 and 10 helices with mesh refinement.

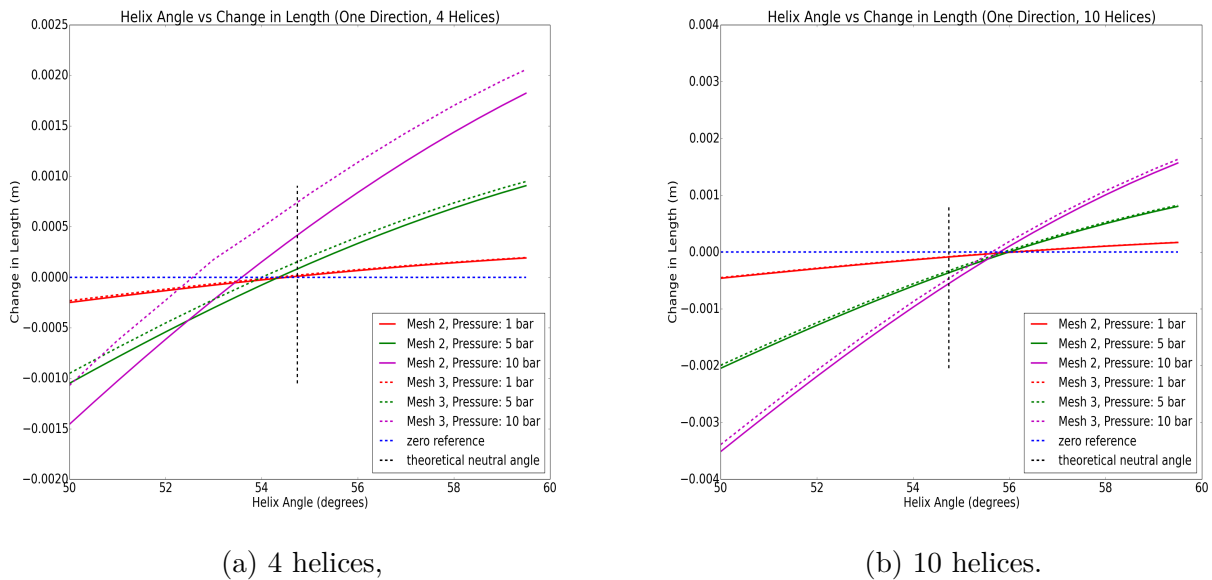


Figure 4.12: Results of coupled model with reinforcement in one direction for varying pressures.

For lower pressures, a mesh convergence has been achieved in both the cases whereas the neutral angle seems to be reducing considerably with increase in pressure for 4 helices case. This is due to the radial expansion of the rubber which would in turn modify the helix angle resulting in the deviation. With 10 helices, the difference in the neutral angle is found to be small. From the results of Figure (4.11) and Figure (4.12), it is evident that with higher number of reinforcements, the neutral angle would remain constant and would not depend on the the pressure level.

The deviation in the neutral angle for the model and the theoretical value can be explained by the dimensions of the rubber hose used which does not satisfy the thin-walled cylinder assumption. The theoretical value is derived using thin-walled cylinder assumption that states that the thickness of the cylinder should not be more than one-tenth of its mean radius. Thus, different geometries have been used to check whether the geometry would cause the deviation.

Table 4.1: Different dimensions of rubber hose and reinforcement used in coupled model.

Geometry	R_o (mm)	R_i (mm)	r (mm)
1	10	9	9.5
2	10	9.5	9.75

The results from the neutral angle simulations using the geometries presented in Table (4.1) for a pressure of 1 bar are shown in Figure (4.13) for 10 and 12 helical reinforcements. It has been observed that with the new geometries that satisfy thin-walled cylinder assumptions, the neutral angle is closer to the theoretical value compared to earlier results. To quantify the values, the neutral angle were found to be closer to 56° in the earlier results and with the new geometries, the neutral angle is closer to 55° .

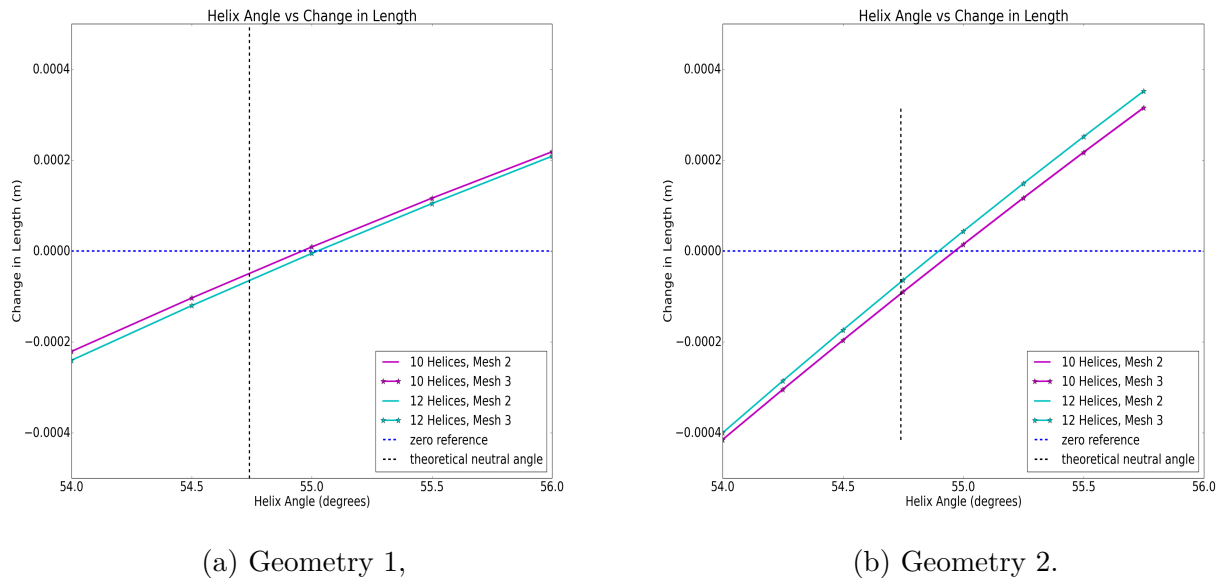


Figure 4.13: Results of coupled model using different geometries.

Based on all the results presented in this Section, the coupled model is found to be working as expected and agrees with the theoretical value.

4.5 Embedded Model - Neutral Angle Simulations

Initially, the mesh intersection algorithm is implemented and the outcome is visualized in Figure (4.14) for one element and the whole model. The following values of the tolerances, that were introduced in Section 3.6.1.3, are found to be suitable as presented in Table (4.2).

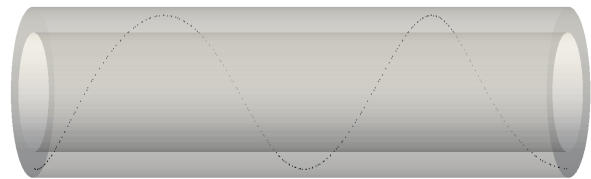
Table 4.2: Tolerance values.

Tolerance	Value
ε_b	$1 \cdot 10^{-12}$
ε_c	$1 \cdot 10^{-7}$
ϵ	$0.05 \cdot \frac{\pi}{180}$

Each black dot in the model are the intersecting points and the nodes for the reinforcement model are positioned at these points.



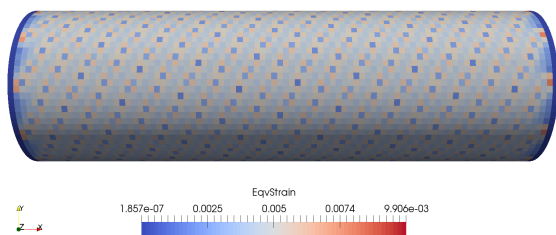
(a) Intersecting points in an element,



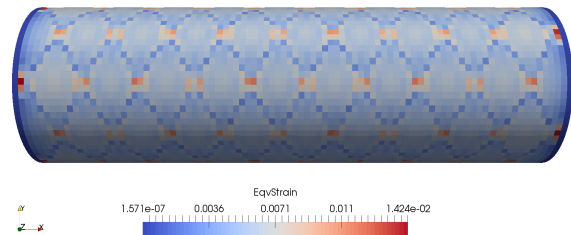
(b) Intersecting points in the whole model.

Figure 4.14: Mesh intersecting points.

The strain contours of the rubber model are presented below.



(a) Reinforcement in one direction,



(b) Reinforcement in two directions.

Figure 4.15: Strain contours of embedded model.

The results from neutral angle simulations for reinforcements in one and two directions for 1 bar pressure are presented below.

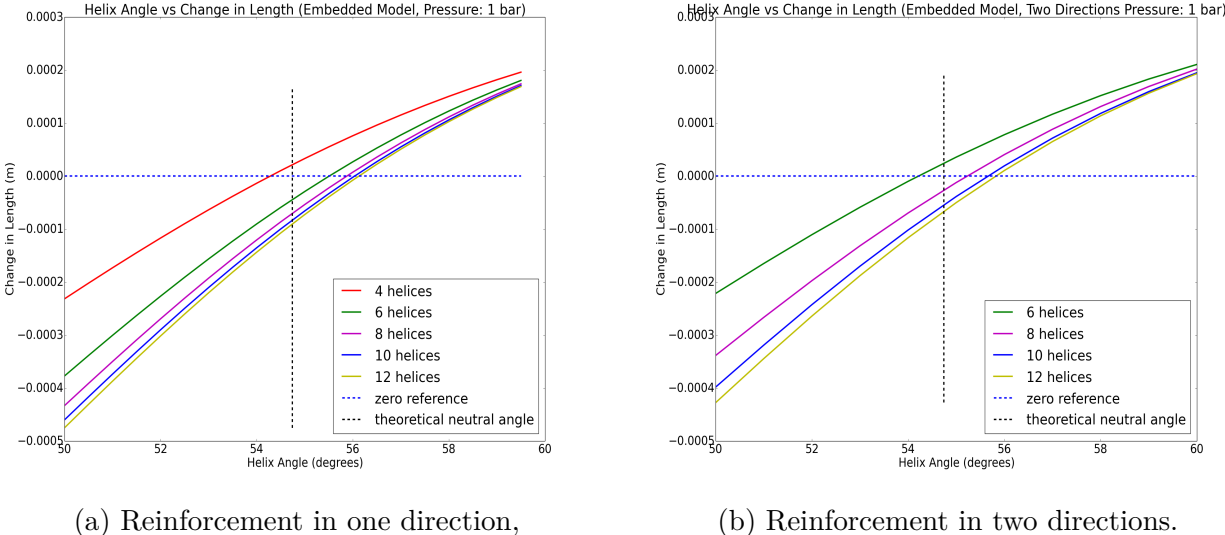


Figure 4.16: Results of embedded model for 1 bar pressure.

The behaviour of embedded model is found to be similar to that of the coupled model. With increasing number of reinforcements, the neutral angle is converging to 56°. Further, the results with geometry 1 as mentioned in Table (4.1), presented in Figure (4.17), shows that the model has good agreement with the theoretical value if it satisfies thin-walled cylinder assumption.

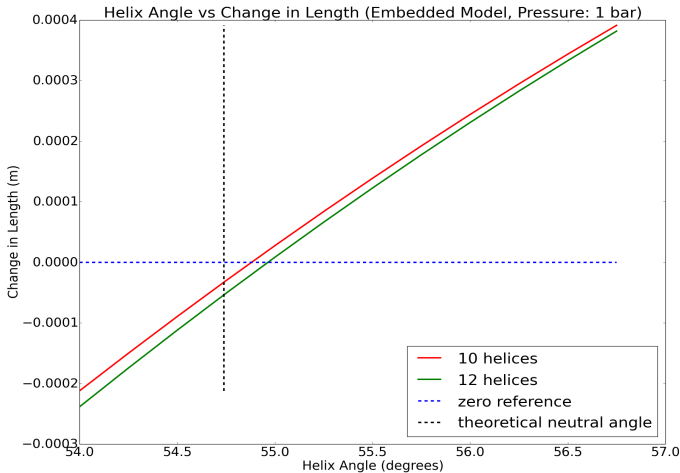


Figure 4.17: Results of embedded model with different geometry.

Thus, the embedded model is found to be working in a reasonable fashion. Note that the embedded model is a linear model in contrast to the coupled model.

4.6 Abaqus Model - Neutral Angle Simulations

A comparison is made between the coupled model and the Abaqus model for pressure levels of 1 bar and 5 bar in a similar study for neutral angle. It is observed that the behaviour is similar for both the models with a slight deviation in the deformation as shown in Figure (4.18). The reason for the difference could be because of the differences in modeling the reinforcements. In the coupled model, the reinforcements are modeled in 1D whereas a 3D model is considered in Abaqus.

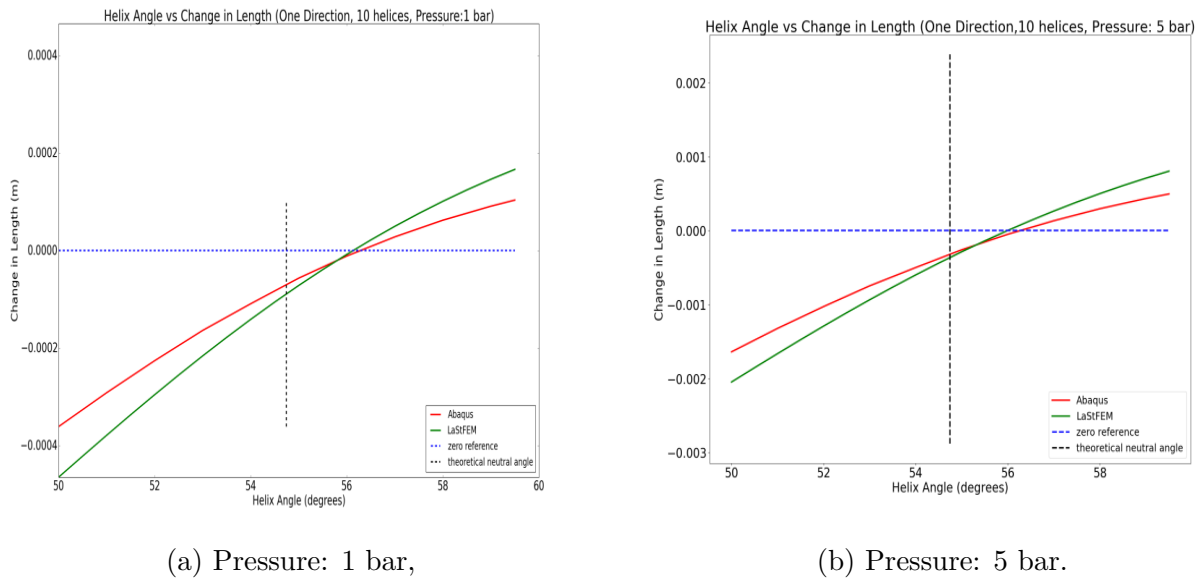


Figure 4.18: Comparison between Abaqus and Coupled models.

4.7 Bending Simulation

4.7.1 Three Point Bending

The setup used and the deformation of the reinforced hose for a pressure of 10 bar are presented in Figure (4.19). The displacement contour is shown on the model along with the deformation. In pressurization, a small displacement due to radial expansion is observed for the reinforced hose. Helix angle of 56° is used since the neutral angle was converging close to it as inferred from Figure (4.10).

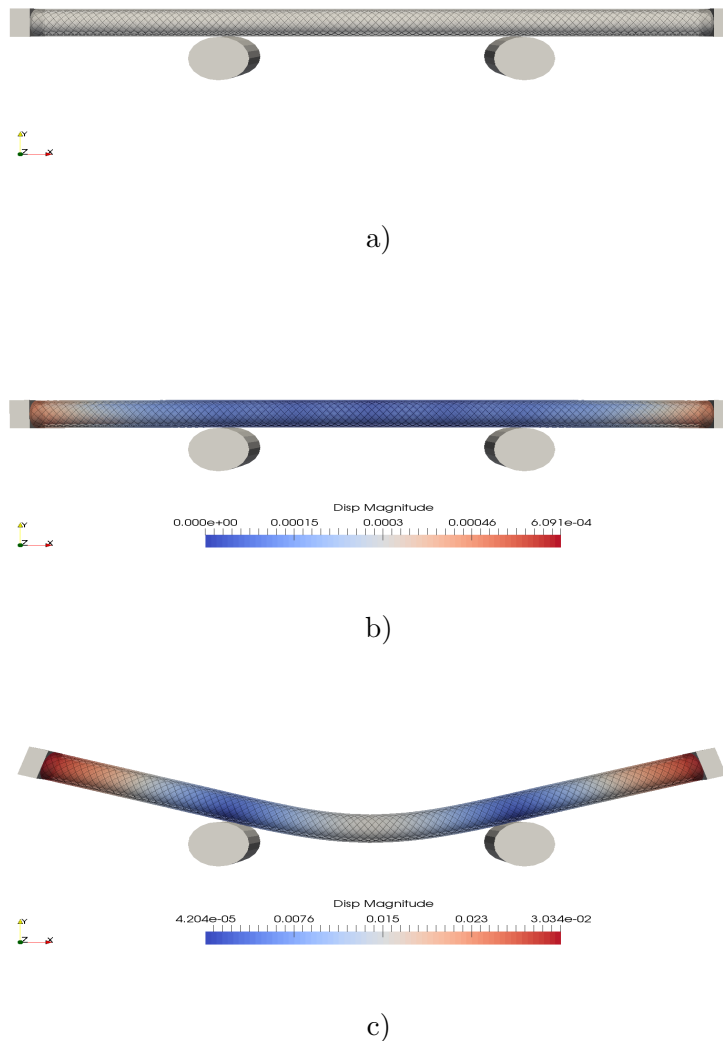


Figure 4.19: Three point bending model setup and deformation. a) Model setup, b) Deformation with displacement magnitude after pressurization step, c) Deformation with displacement magnitude after displacement steps.

The results from three point bending simulations with a comparison between pure rubber hose model and reinforced hose model for varying pressures can be seen in Figure (4.20). It can be observed that the rubber hose gets stiffer with higher pressure levels. Also, for 0 bar pressure, the reinforced hose requires higher reaction forces than the rubber hose and with higher pressures, both the reinforced hose and rubber hose seems to require similar forces. The reaction force values at 0 m displacement are the force values extracted after pressurization step. For higher pressures, a non-zero reaction force is seen for rubber hose which is due to the restriction of the radial expansion because of the boundary condition and the presence of the supports.

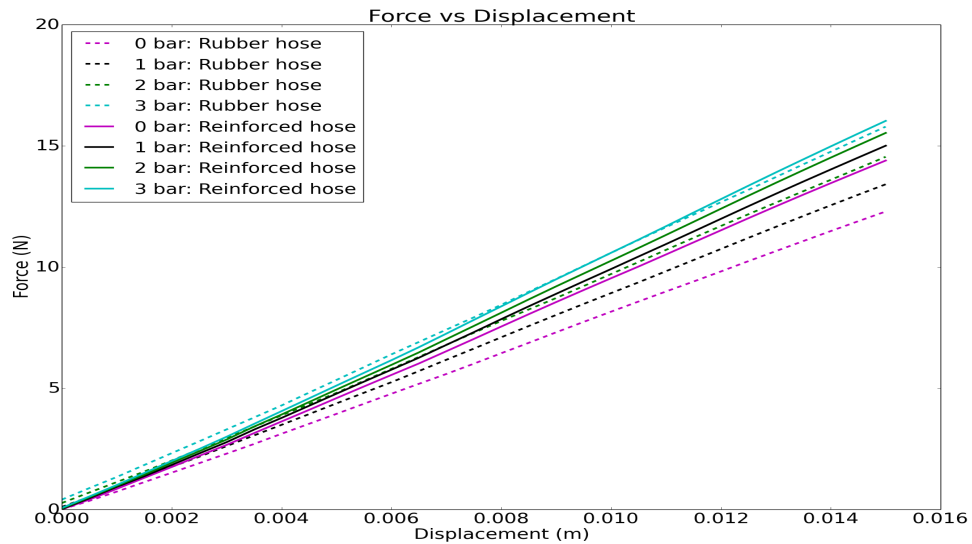


Figure 4.20: Results from three point bending simulations for varying pressures.

To investigate the cause for the increased stiffness for rubber hose model, the radial deformation as an effect of pressurization is studied. The strain contours of a rubber hose model and a reinforced hose model for a 3 bar pressure are presented in Figure (4.21).

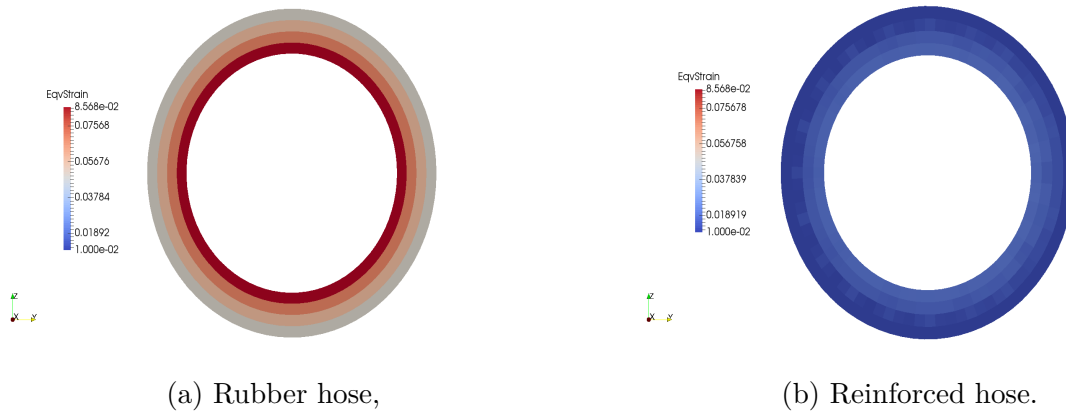


Figure 4.21: Strain contours on the cross section after pressurization step.

It is noted that there is a considerable expansion in the rubber hose model whereas a very minimal change is observed in the reinforced hose model. Thus, the increased stiffness detected in the rubber hose could be because of the increase in the moment of inertia caused by the radial expansion. To study this further, the bending stiffness (EI) is derived from Equation (3.56) (denoted as method 1 in the Figure (4.22)) using the reaction force values from the simulation and compared with the value of EI found by multiplying the Young's modulus of rubber with an updated moment of inertia determined from Equation (3.57) using the

new radius of the hose after pressurization (denoted as method 2). The results from the comparison are presented in Figure (4.22) in which the bending stiffness values are plotted against pressure level. From

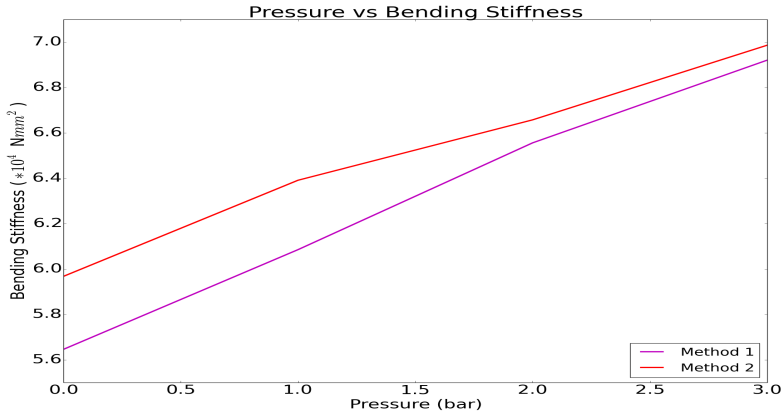


Figure 4.22: Comparison of bending stiffness.

the comparison, it is clearly seen that the bending stiffness values determined directly from the simulation agrees well with the bending stiffness values determined using increased moment of inertia. It can be concluded that, increased bending stiffness in the rubber hose is due to an increased moment of inertia.

The three point bending simulations are performed for higher pressures for the reinforced hose with 10 helical reinforcements and 20 helical reinforcements to analyze if there is an increase in the stiffness with more number of reinforcements. The results are presented in Figure (4.23).

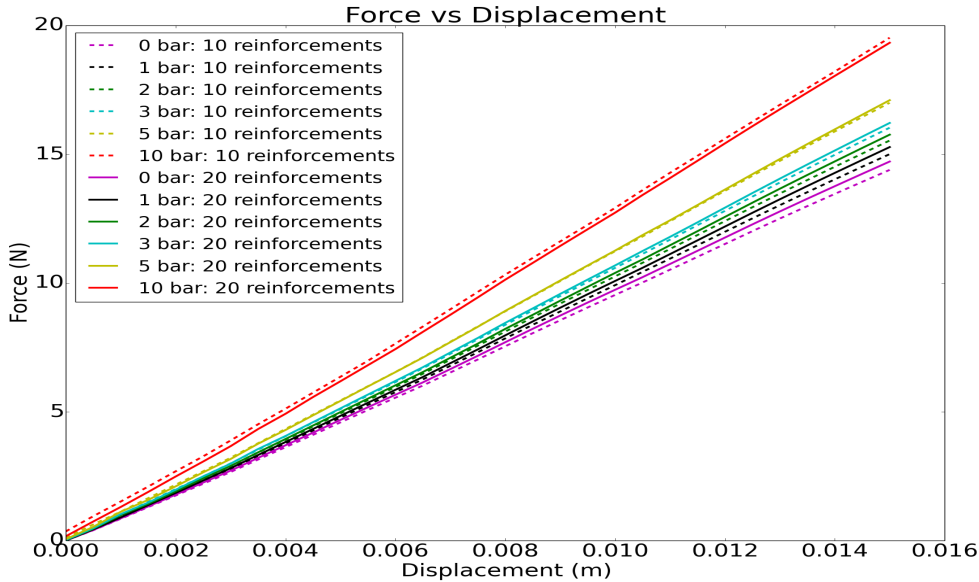


Figure 4.23: Results from three point bending simulations for reinforced hose model.

4. Results & Discussions

It is observed at lower pressure levels, higher reaction forces are required for reinforced hose with 20 reinforcements. However, for a pressure of 10 bar, reinforced hose with 10 reinforcements require higher reaction forces. Even though the radial deformation is minimal, reinforced hose with 10 reinforcements deforms more when compared to a reinforced hose with 20 reinforcements causing this difference. Note that, for 10 bar, a higher reaction force is detected after pressurization. To compare bending stiffness, Equation (3.56) is used to derive EI value as performed in method 1 earlier. The results are presented in Figure (4.24) with a comparison with rubber hose for lower pressures and between the reinforced hoses alone for higher pressures.

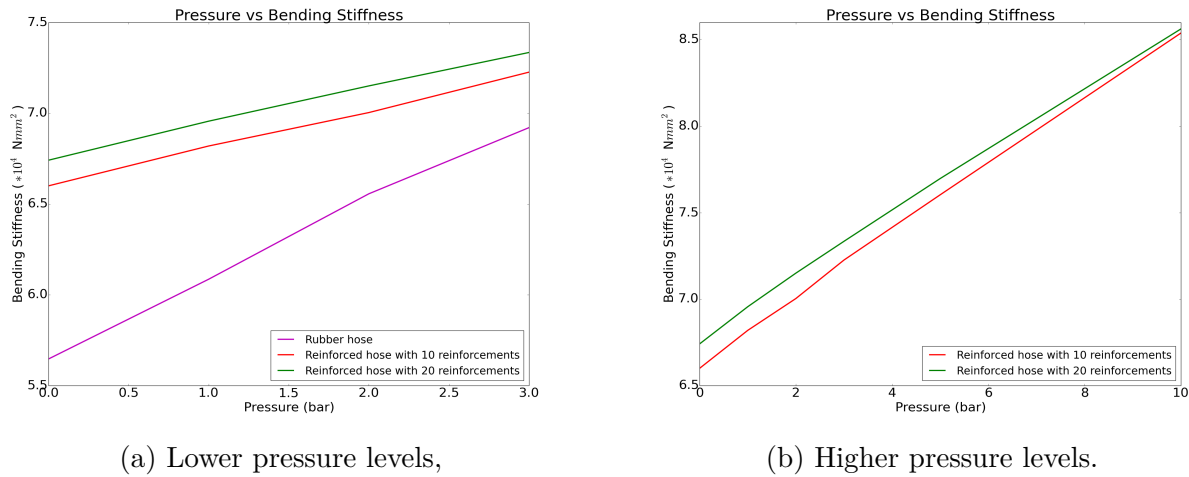


Figure 4.24: Comparison of bending stiffness vs pressure for different models.

The results show that the reinforced hose have higher bending stiffness compared to a rubber hose and that the bending stiffness increases for the reinforced hose with more reinforcements. An effective value of the Young's modulus of hoses can be determined from a 0 bar case through division of the bending stiffness value by the moment of inertia which would be the same for rubber and reinforced hose and has been tabulated in Table (4.3).

Table 4.3: Effective Young's modulus of reinforced hose.

Value/Model	Rubber	Reinforced with 10 reinforcements	Reinforced with 20 reinforcements
E (MPa)	9.2310	11.0586	11.2951

With higher pressure levels, since the radial deformation is very minimal for a reinforced hose, the increase in bending stiffness can be attributed due to the presence of the reinforcements. Further, from the results, it can be concluded that the bending stiffness of the reinforced hose model increase with higher pressures.

4.7.2 MeSOMICS

The FE model setup for constrained pressurization and unconstrained pressurization and the corresponding deformation after pressurization step and displacement steps are shown in Figure (4.25). The displacement in the rubber model after pressurization is denoted in the contours. The difference between the setups is visible in Figures (4.25) (c) and (d). In setup 2, the model is free to translate axially during pressurization steps which results in the displacement.

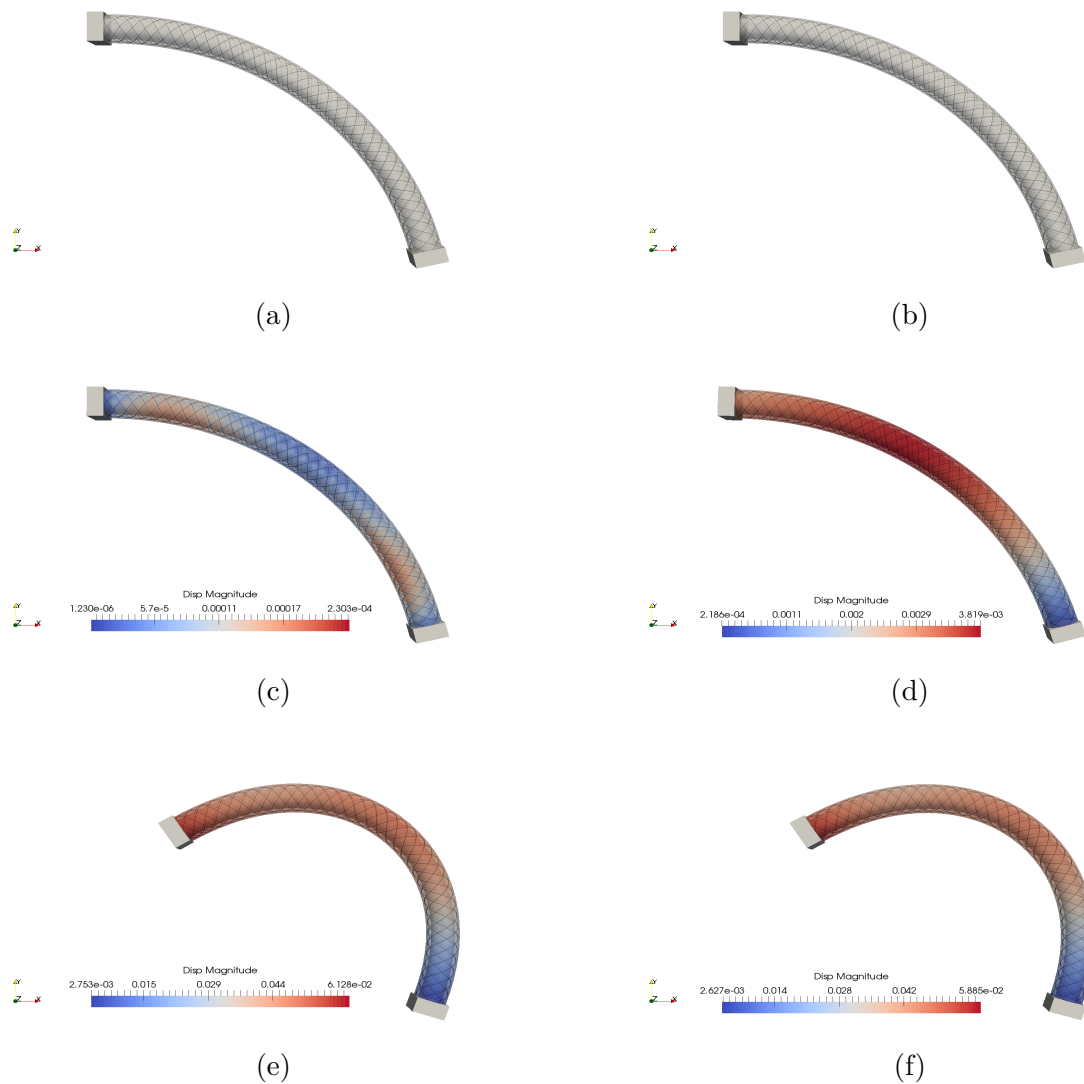


Figure 4.25: Bending model setup and deformation. a) Model setup 1: constrained pressurization , b) Model setup 2: unconstrained pressurization, c) Deformation with displacement magnitude after pressurization step for setup 1, d) Deformation with displacement magnitude after pressurization step for setup 2, e) Deformation with displacement magnitude after displacement steps for setup 1, f) Deformation with displacement magnitude after displacement steps for setup 2.

The results from setup 1 for a hose with 10 helical reinforcements in two directions for different pressure levels are presented in Figure (4.26). Helix angle of 56° is used in this case also since the neutral angle was converging close to it as inferred from Figure (4.10).

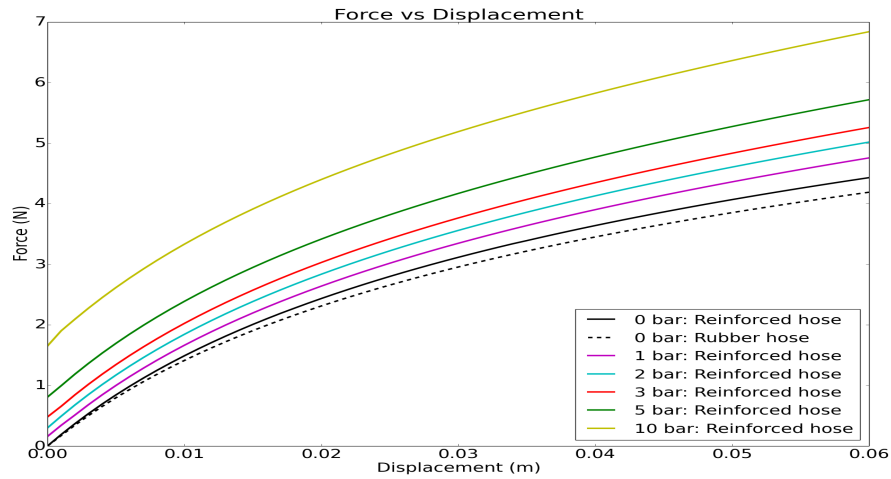


Figure 4.26: Results from Bending Simulations (Setup 1: constrained pressurization).

It is found that, since the slope does not vary, the stiffness remains constant for different pressure levels. With increase in pressure, higher reaction forces are measured after pressurization as an effect of the end forces and boundary condition. The behaviour could be a result of the curvature of the reinforcements. Further, a comparison has been made with a pure rubber hose model for different helix angles. Changing the helix angle would change the total length of the model in each case since the number of revolutions is kept constant for all models. The result from the comparison using setup 2 is given below in Figure (4.27).

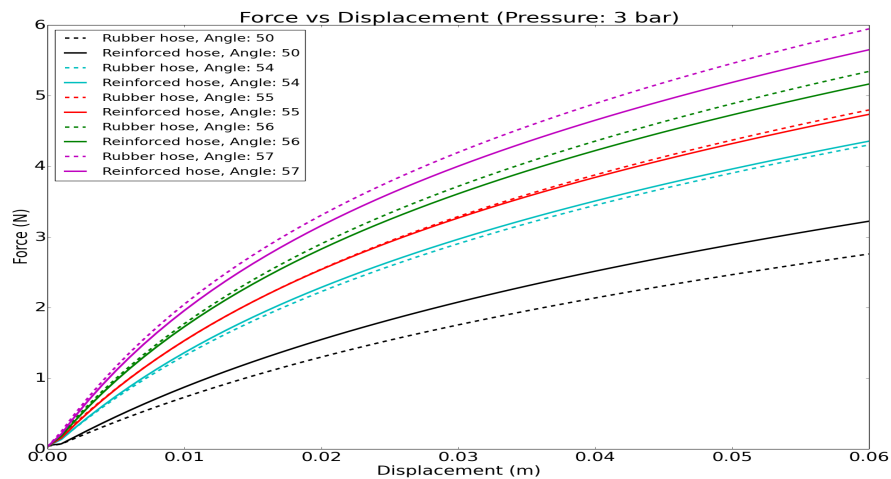


Figure 4.27: Results from Bending Simulations (Setup 2: unconstrained pressurization).

Note that, since the hose is free to expand during pressurization, the starting force is 0 in the plot. It is observed that the helix angle affects the force required. For angles higher than the neutral angle, the reinforced hose shows lower bending stiffness and for angles lesser than the neutral angle, reinforced hose shows higher bending stiffness compared to a pure rubber model.

4.8 Torsion Simulation

The deformation of the model after pressurization and at the end of torsion steps are presented in Figure (4.28). During pressurization, the model is free to translate at one end which results in small displacements as seen in figure (a). A comparison is made between the reinforced hose and the pure rubber hose models

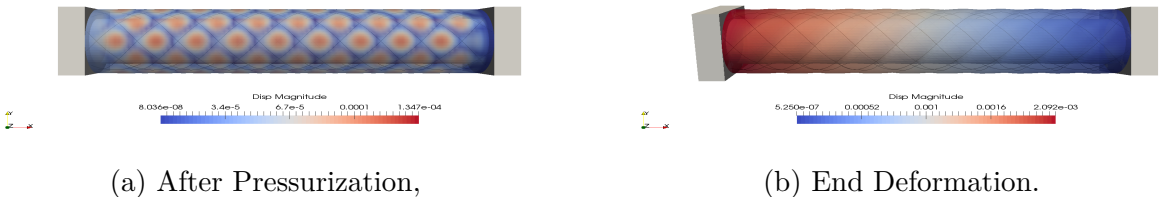


Figure 4.28: Torsion model deformation.

at 0, 1 and 3 bars of pressure. It can be seen from Figure (4.29) that the reinforced hoses are significantly stiffer than rubber hoses which is expected. The results also show that the reinforced hose can maintain higher moments with 1 and 3 bars of pressure.

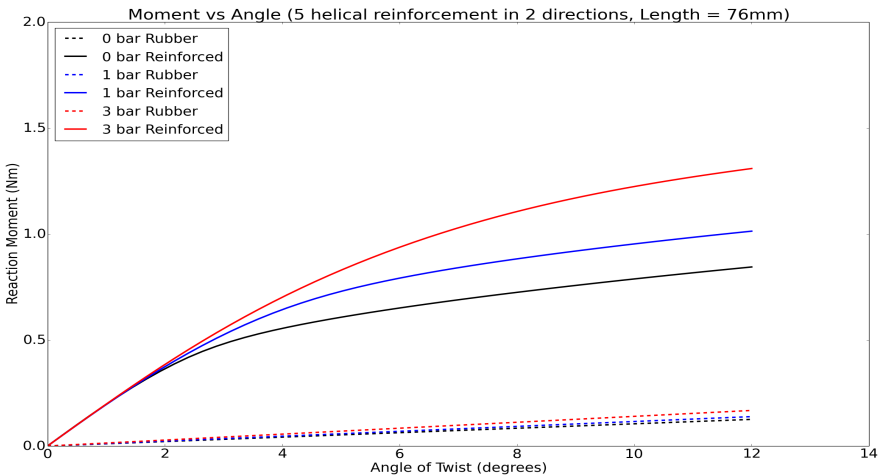


Figure 4.29: Results from Torsion Simulations.

Additionally, the reinforced hoses are simulated for higher pressure levels and the results are presented in Figure (4.30). It can be inferred that, the torsional stiffness is increasing with increase in pressure and

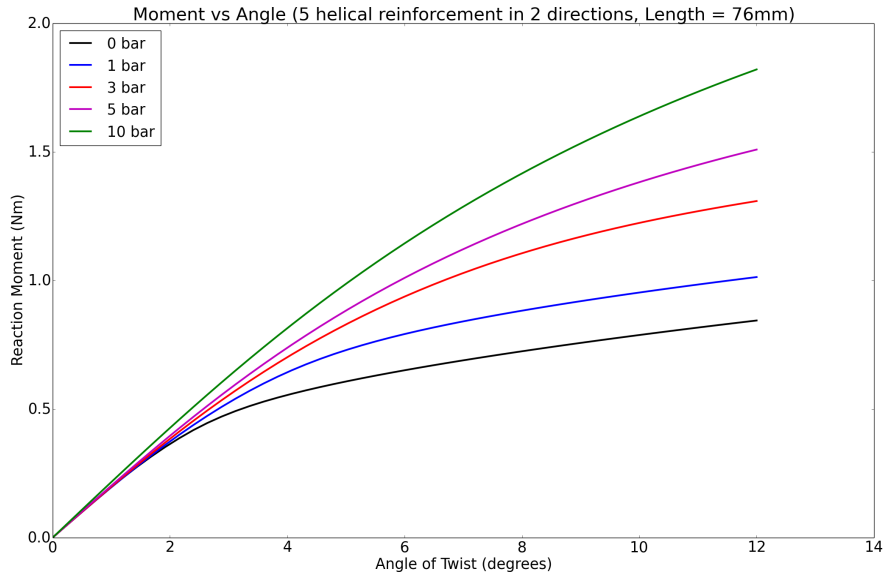


Figure 4.30: Results from Torsion Simulations for higher pressures.

seem to converge to an almost linear behaviour for higher pressure. The presence of reinforcements makes the model harder to twist and the increase in stiffness is due to the increased tension in the reinforcements. With increase in pressure, the reinforcements are subjected to higher tension forces which increases the torsional stiffness of the model. Based on these results, it can be concluded that the coupled model has the capabilities to capture a dependency of torsional stiffness on pressure level.

5

Conclusions & Future Work

5.1 Conclusions

Modeling of helical reinforcements in a hydraulic hose was the main interest in the thesis. At first, helical reinforcements alone were modeled without considering the rubber hose. A beam model was setup using the in-house solver LaStFEM. The results from the beam model for neutral angle simulations reveals that the model was able to predict the effect of neutral angle and showed very good agreement with the theoretical value irrespective of pressure applied. Further, truss elements were considered as an alternative to model reinforcements. The element forces and stiffness contributions were formulated and added as user-defined elements in LaStFEM. The truss model was also found to capture the effect of neutral angle accurately and in correspondence with the theoretical value.

A simplified volume model was considered to model reinforced hose. A cylindrically structured mesh was transformed such that nodes were positioned in a helical fashion. Multiple rows of elements were picked and given steel properties as input to represent helical reinforcements. The model has several limitations but it could predict the effect of a neutral angle. Additionally, a spring coupling was introduced between a truss model of reinforcement and a volume model of rubber hose. The performance of the model was evaluated for different pressure levels and the results were found to be satisfactory and in acceptance with the theoretical value of neutral angle. Furthermore, an embedded model was implemented with the help of a mesh intersection algorithm. Although, the embedded model contribution is a linear model, it was able to predict the neutral angle and had similar behaviour like the coupled model. In both the models, with increasing number of reinforcements, the neutral angle was converging towards a value close to 56° . It was found that if the dimensions of the rubber model satisfies the thin-walled cylinder assumption, the neutral angle obtained was very close to the theoretical value. The hydraulic hose was also modeled in Abaqus using an embedded constraint considering a 3D model for both the rubber hose and the reinforcement. The behaviour was found to be similar to the coupled model.

Finally, the behaviour of the coupled model was studied in bending and in torsion. To study bending, three point bending and MeSOMICS methods are used. From the results of the three point bending simulation, the bending stiffness was found to be increasing with higher pressures. The stiffness was also observed to be increasing for rubber hose models but it was found that there is a considerable radial expansion which causes an increase in moment of inertia. In MeSOMICS simulations, the reinforced hose was found to be stiffer than the rubber hose but the bending stiffness of the reinforced hose was not increasing with

pressure which could be a result of the curvature of the reinforcements. Also, changing the helix angle in unconstrained pressurization setup had an effect on the bending stiffness of the reinforced hose due to the change in length after pressurization. For angles higher than the neutral angle, the reinforced hose shows lower bending stiffness and for angles lesser than the neutral angle, reinforced hose shows higher bending stiffness compared to a pure rubber model.

Results from torsion simulation demonstrates that the torsional stiffness of the reinforced hose model is significantly higher than a pure rubber hose model. Moreover, the torsional stiffness was found to be increasing with pressure. The main reason being that the reinforcements are subjected to higher tension forces with higher pressures.

5.2 Future Work

Due to time constraints, other alternatives such as higher pressures with more reinforcements or different curvatures could not be tried out in MeSOMICS simulations for which there could be a change in stiffness. These alternatives can be worked upon next.

Further, reinforcements could be modeled in multiple layers which could be validated with the analytical results of Entwistle [6]. The interactions between the reinforcements and the friction effects between the reinforcements and the rubber could be a key factor in capturing the increased stiffness in bending. Thus, modeling these contributions should ideally be the next step. If a non-linear approach is derived for the embedded method, it would also be possible to use that model to study bending and torsion.

Bibliography

- [1] J. Reddy, *Introduction to the Finite Element Method*. McGraw-Hill, 1993, ISBN: 9780070513563. [Online]. Available: <https://books.google.se/books?id=2NOIPwAACAAJ>.
- [2] E. W. Weisstein, “Helix.”, *From MathWorld—A Wolfram Web Resource*. <http://mathworld.wolfram.com/Helix.html>, 2003.
- [3] H. F. Subcommittee, “Wire braid angle response characteristics in hydraulic hose”, *SAE Transaction*, vol. 972706, pp. 107–126, 1997.
- [4] B. Van den Horn and M. Kuipers, “Strength and stiffness of a reinforced flexible hose”, *Applied scientific research*, vol. 45, no. 3, pp. 251–281, 1988.
- [5] K. Entwistle and G. White, “A method for achieving effective load transfer between the inner and outer layers of a two-layer braided high-pressure hydraulic hose”, *International Journal of Mechanical Sciences*, vol. 19, no. 4, pp. 193–201, 1977.
- [6] K. Entwistle, “The behaviour of braided hydraulic hose reinforced with steel wires”, *International Journal of Mechanical Sciences*, vol. 23, no. 4, pp. 229–241, 1981.
- [7] P. Bregman, M. Kuipers, H. Teerling, and W. Van der Veen, “Strength and stiffness of a flexible high-pressure spiral hose”, *Acta mechanica*, vol. 97, no. 3-4, pp. 185–204, 1993.
- [8] J. Crossley, A. Spencer, and A. England, “Analytical solutions for bending and flexure of helically reinforced cylinders”, *International Journal of Solids and Structures*, vol. 40, no. 4, pp. 777–806, 2003.
- [9] F. Gu, C.-k. Huang, J. Zhou, and L.-p. Li, “Mechanical response of steel wire wound reinforced rubber flexible pipe under internal pressure”, *Journal of Shanghai Jiaotong University (Science)*, vol. 14, no. 6, p. 747, 2009.
- [10] L. Frérot, “Developing a 3d finite element model for reinforced concrete”, Tech. Rep., 2015.
- [11] B. Lé, G. Legrain, and N. Moës, “Mixed dimensional modeling of reinforced structures”, *Finite Elements in Analysis and Design*, vol. 128, pp. 1–18, 2017, ISSN: 0168-874X. DOI: <https://doi.org/10.1016/j.finel.2017.01.002>. [Online]. Available: <http://www.sciencedirect.com/science/article/pii/S0168874X16301184>.
- [12] T. Y. Chang, M. ASCE, H. Taniguchi, and W. F. Chen, “Nonlinear finite element analysis of reinforced concrete panels”, *Journal of Structural Engineering*, vol. 113, 1 1987.
- [13] A. Llau, L. Jason, F. Dufour, and J. Baroth, “Finite element modelling of 1d steel components in reinforced and prestressed concrete structures”, *Engineering Structures*, vol. 127, pp. 769–783, 2016, ISSN: 0141-0296. DOI: <https://doi.org/10.1016/j.engstruct.2016.09.023>. [Online]. Available: <http://www.sciencedirect.com/science/article/pii/S0141029616305909>.
- [14] D. M. Ian, I. W. Doherty, D. M. Court, and C. G. Armstrong, “Coupling 1d beams to 3d bodies”, pp. 285–293, 1998.
- [15] M. Sadek and I. Shahrou, “A three dimensional embedded beam element for reinforced geomaterials”, *International Journal for Numerical and Analytical Methods in Geomechanics*, vol. 28, no. 9, pp. 931–

- 946, 2004. DOI: [10.1002/nag.357](https://doi.org/10.1002/nag.357). eprint: <https://onlinelibrary.wiley.com/doi/pdf/10.1002/nag.357>. [Online]. Available: <https://onlinelibrary.wiley.com/doi/abs/10.1002/nag.357>.
- [16] D. F. Turello, F. Pinto, and P. J. Sánchez, “Embedded beam element with interaction surface for lateral loading of piles”, *International Journal for Numerical and Analytical Methods in Geomechanics*, vol. 40, no. 4, pp. 568–582, 2016. DOI: [10.1002/nag.2416](https://doi.org/10.1002/nag.2416). eprint: <https://onlinelibrary.wiley.com/doi/pdf/10.1002/nag.2416>. [Online]. Available: <https://onlinelibrary.wiley.com/doi/abs/10.1002/nag.2416>.
- [17] J. Ninić, J. Stascheit, and G. Meschke, “Beam–solid contact formulation for finite element analysis of pile–soil interaction with arbitrary discretization”, *International Journal for Numerical and Analytical Methods in Geomechanics*, vol. 38, no. 14, pp. 1453–1476, 2014. DOI: [10.1002/nag.2262](https://doi.org/10.1002/nag.2262). eprint: <https://onlinelibrary.wiley.com/doi/pdf/10.1002/nag.2262>. [Online]. Available: <https://onlinelibrary.wiley.com/doi/abs/10.1002/nag.2262>.
- [18] W. Breig, “Finite element analysis of spiral hose utilizing laminate theory”, *SAE transactions*, pp. 968–986, 1991.
- [19] J. Cho, Y. Jee, W. Kim, S. Han, and S. Lee, “Homogenization of braided fabric composite for reliable large deformation analysis of reinforced rubber hose”, *Composites Part B: Engineering*, vol. 53, pp. 112–120, 2013.
- [20] *LaStFEM.*, [Online]. Available: <http://www.fcc.chalmers.se/technologies/comp/computational-structural-dynamics/>.
- [21] T. Belytschko, W. Liu, and B. Moran, *Nonlinear Finite Elements for Continua and Structures*, English. John Wiley & Sons, Ltd, 2000.
- [22] A. Forslund, S. Lorin, L. Lindkvist, K. Wärmefjord, and R. Söderberg, “Minimizing weld variation effects using permutation genetic algorithms and virtual locator trimming”, *Journal of Computing and Information Science in Engineering*, vol. 18, no. 4, p. 041 010, 2018.
- [23] S. Lorin, C. Cromvik, F. Edelvik, L. Lindkvist, and R. Söderberg, “On the robustness of the volumetric shrinkage method in the context of variation simulation”, in *ASME 2014 International Mechanical Engineering Congress and Exposition*, American Society of Mechanical Engineers, 2014, V02AT02A053–V02AT02A053.
- [24] —, “Variation simulation of welded assemblies using a thermo-elastic finite element model”, *Journal of Computing and Information Science in Engineering*, vol. 14, no. 3, p. 031 003, 2014.
- [25] S. Lorin, C. Cromvik, F. Edelvik, L. Lindkvist, R. Söderberg, and K. Wärmefjord, “Simulation of non-nominal welds by resolving the melted zone and its implication to variation simulation”, in *ASME 2014 International Design Engineering Technical Conferences and Computers and Information in Engineering Conference*, American Society of Mechanical Engineers, 2014, V004T06A018–V004T06A018.
- [26] S. Lorin, C. Cromvik, F. Edelvik, and R. Söderberg, “Welding simulation of non-nominal structures with clamps”, *Journal of Computing and Information Science in Engineering*, vol. 15, no. 2, p. 021 004, 2015.
- [27] M. et al, “A virtual design of experiments method to evaluate the effect of design and welding parameters on weld quality in aerospace applications”, *Journal of Aerospace Manufacturing*, 2019.
- [28] E. Svenning, A. Mark, and F. Edelvik, “Simulation of a highly elastic structure interacting with a two-phase flow”, *Journal of Mathematics in Industry*, vol. 4, no. 1, p. 7, 2014.
- [29] E. Svenning, A. Mark, F. Edelvik, E. Glatt, S. Rief, A. Wiegmann, L. Martinsson, R. Lai, M. Fredlund, and U. Nyman, “Multiphase simulation of fiber suspension flows using immersed boundary methods”, *Nordic Pulp & Paper Research Journal*, vol. 27, no. 2, pp. 184–191, 2012.

-
- [30] C. Jareteg, K. Wärmefjord, R. Söderberg, L. Lindkvist, J. Carlson, C. Cromvik, and F. Edelvik, “Variation simulation for composite parts and assemblies including variation in fiber orientation and thickness”, *Procedia CIRP*, vol. 23, pp. 235–240, 2014.
- [31] C. Jareteg, K. Wärmefjord, C. Cromvik, R. Söderberg, L. Lindkvist, J. Carlson, S. Larsson, and F. Edelvik, “Geometry assurance integrating process variation with simulation of spring-in for composite parts and assemblies”, *Journal of Computing and Information Science in Engineering*, vol. 16, no. 3, p. 031003, 2016.
- [32] M. Smith, *ABAQUS/Standard User’s Manual, Version 6.13*, English. Simulia.
- [33] Singiresu.S.Rao, *The Finite Element Method in Engineering*. Elsevier, 2011, ISBN: 9781856176613.
- [34] R. Durand, M. M. Farias, and D. M. Pedroso, “Computing intersections between non-compatible curves and finite elements”, *Computational Mechanics*, vol. 56, no. 3, pp. 463–475, 2015, ISSN: 1432-0924. DOI: [10.1007/s00466-015-1181-y](https://doi.org/10.1007/s00466-015-1181-y). [Online]. Available: <https://doi.org/10.1007/s00466-015-1181-y>.
- [35] *MeSOMICS*, [Online]. Available: <https://www.itwm.fraunhofer.de/en/departments/mdf/nonlinear-structural-mechanics/mesomics-ips-cable-simulation.html>.